P 2mit

NASA TECHNICAL NOTE

NASA TN D-7615

NASA TN D-7615

(NASA-TN-D-7615) COMPARISON OF ISOTHERMAL AND CYCLIC OXIDATION BEHAVIOR OF TWENTY-FIVE COMMERCIAL SHEET ALLOYS AT 1150 C (NASA) 52 p HC $3.75 CSCL 11D

N74-21134

Unclas
H1/17 36038

MAY 1974
RECEIVED
NASA STI FACILITY
INPUT BRANCH

COMPARISON OF ISOTHERMAL AND CYCLIC OXIDATION BEHAVIOR OF TWENTY-FIVE COMMERCIAL SHEET ALLOYS AT 1150° C

by Charles A. Barrett and Carl E. Lowell

Lewis Research Center
Cleveland, Ohio 44135

NATIONAL AERONAUTICS AND SPACE ADMINISTRATION • WASHINGTON, D. C. • APRIL 1974

1. Report No.	2. Government Accession No.	3. Recipient's Catalog No.
NASA TN D-7615		

4. Title and Subtitle	5. Report Date
COMPARISON OF ISOTHERMAL AND CYCLIC OXIDATION BEHAVIOR OF TWENTY-FIVE COMMERCIAL SHEET ALLOYS AT 1150° C	APRIL 1974
	6. Performing Organization Code

7. Author(s)	8. Performing Organization Report No.
Charles A. Barrett and Carl E. Lowell	E-7629
	10. Work Unit No. 501-01

9. Performing Organization Name and Address	11. Contract or Grant No.
Lewis Research Center National Aeronautics and Space Administration Cleveland, Ohio 44135	
	13. Type of Report and Period Covered Technical Note

12. Sponsoring Agency Name and Address	14. Sponsoring Agency Code
National Aeronautics and Space Administration Washington, D. C. 20546	

15. Supplementary Notes

16. Abstract

The cyclic and isothermal oxidation resistance of 25 high-temperature Ni-, Co-, and Fe-base sheet alloys after 100 hours in air at 1150° C was compared. The alloys were evaluated in terms of their oxidation, scaling, and vaporization rates and their tendency for scale spallation. These values were used to develop an oxidation rating parameter based on effective thickness change, as calculated from a mass balance. The calculated thicknesses generally agreed with the measured values, including grain boundary oxidation, to within a factor of 3. Oxidation behavior was related to composition, particularly Cr and Al content.

17. Key Words (Suggested by Author(s))	18. Distribution Statement
Isothermal oxidation; Cyclic oxidation; Scaling; Oxide spalling; Heater alloys; Superalloy sheet; TD-alloys; Oxide vaporization; NiCrAl alloys; CoCr alloys; NiCr alloys;	Unclassified - unlimited CAT. 17

19. Security Classif. (of this report)	20. Security Classif. (of this page)	21. No. of Pages	22. Price*
Unclassified	Unclassified	52	$3.75

* For sale by the National Technical Information Service, Springfield, Virginia 22151

COMPARISON OF ISOTHERMAL AND CYCLIC OXIDATION BEHAVIOR OF TWENTY-FIVE COMMERCIAL SHEET ALLOYS AT 1150° C

by Charles A. Barrett and Carl E. Lowell

Lewis Research Center

SUMMARY

Twenty-five commercial nickel-, iron-, and cobalt-base sheet alloys incorporating chromium or chromium and aluminum additions for oxidation resistance were tested at 1150° C in air for 100 hours in both isothermal and 1-hour cyclic furnace exposures. The alloys were evaluated by sample specific weight change, by type of scale formed, by amount and type of spall, and by sample thickness change and microstructure.

In isothermal steady-state oxidation, four types of controlling oxides were observed depending on alloy composition: NiO, Cr_2O_3/chromite spinel, ThO_2-blocked Cr_2O_3, and αAl_2O_3/aluminate spinel. The latter three types are considered protective. In the Cr_2O_3-forming alloys, however, scale vaporization is a critical factor in determining the parabolic scaling rate based on paralinear oxidation. In cyclic oxidation the alloys which form Cr_2O_3/chromite spinel scales were degraded severely when sufficient chromite spinel developed to trigger spalling. The cyclic behavior of the other three types of alloys does not differ greatly from their isothermal behavior. If chromite spinel formation is minimal, the thinner the oxide formed, the less the tendency to spall. Factors contributing to a thin scale are low isothermal scaling rates; reactive element additions, such as thorium, lanthanum, and silicon; and scale vaporization. Scale vaporization may, however, lead to catastrophic oxidation at high gas velocities and/or low pressures.

A tentative mass-balance approach to scale buildup, scale vaporization, and scale spalling was used to calculate the critical oxidation parameter - the effective metal thickness change. In general, this calculated thickness change agrees with the measured change to within a factor of 3 if a correction is made for grain boundary oxidation. The

calculated thickness change parameter was used to rate the oxidation resistance of the various alloys under isothermal or cyclic conditions. The best alloys in cyclic furnace oxidation tests were either αAl_2O_3/aluminate spinel formers or Cr_2O_3 formers with ThO_2 blockage.

INTRODUCTION

Iron, nickel, and cobalt sheet alloys that have good oxidation resistance above 1100° C have potential for a wide variety of aerospace applications including gas turbine combustors, claddings for less-oxidation-resistant airfoil materials, and heat shields for reentry vehicles. These alloys depend mainly on their chromium or chromium and aluminum contents to form protective scales. The literature contains considerable isothermal oxidation data for such materials. Those data have been used to calculate oxidation rate constants, activation energies of the oxidation reaction, and so forth. (Ref. 1 is the most recent summary of such studies.) Alloys high in chromium tend to confer protection by forming Cr_2O_3 which, however, has significant volatility at 1100° C and above (ref. 2). Except for TD-NiCr (ref. 3) the role of Cr_2O_3 volatility in the oxidation behavior of commercial alloys has been little investigated. In addition, few studies have examined the high-temperature cyclic oxidation behavior of sheet alloys even though actual usage generally involves frequent cycles between ambient and service temperatures. For this reason, 25 selected iron, nickel, and cobalt sheet alloys were laboratory tested at 1150° C using 1-hour exposures at temperature. The specific weight change, spall weight, thickness change, and scale/spall composition data obtained were compared to similar isothermal test data.

The purposes of this study were as follows:

(1) To characterize in detail the isothermal oxidation behavior of the alloys studied, including which oxide controls the scaling reaction and the role of the critical alloying elements (Cr or Cr and Al) and emphasizing the role of Cr_2O_3 vaporization

(2) To test the same alloys in cyclic oxidation, to compare them to each other, and to compare the results to the isothermal results

(3) To attempt to develop a nondestructive method of estimating sample thickness change based on weight change data so the oxidation resistance of the alloys can be compared regardless of how they are tested - cyclically or isothermally

PROCEDURE

Materials

Test coupons 1.27 centimeters by 1.90 centimeters, and generally 1 to 3 millimeters thick, with a 0.318-centimeter-diameter hanger hole were cut from as-received sheet. The alloys tested are classified as to type in table I and listed with their chemical composition and thicknesses. Prior to testing, the samples were degreased and ultrasonically cleaned, measured with a micrometer to the nearest 0.001 millimeter, and weighed to the nearest 0.1 milligram.

Isothermal Oxidation

Isothermal tests at 1150° C were conducted by suspending the sample from the bottom of an automatic recording balance into a resistance-wound vertical tube furnace at 1150° C and exposing them for 100 hours. This test setup is shown in figure 1. The temperature was controlled to within 1 percent. Since the bottom of the furnace was closed, the air was essentially still with only natural convection occurring. The weight change was recorded continuously and read to the nearest 0.1 milligram to generate curves of specific weight change ($\Delta W/A$) against time. Hereinafter this specific weight change will be termed ΔW. At the end of 100 hours the furnace was lowered and the suspended sample was surrounded with a beaker to catch the spall as the sample cooled.

Cyclic Oxidation

Other test samples were exposed at 1150° C (controlled to within 1 percent) for 100 heating cycles of 1 hour each. A typical sample's heating and cooling rate curve is given in figure 2. Between each exposure cycle the sample was cooled to room temperature for a minimum of 40 minutes. The samples were suspended in individual ceramic tubes of a vertical tube furnace. The furnace consisted of six 2.86-centimeter-diameter alumina tubes symmetrically arranged around the inner circumference of a 12.7-centimeter-diameter Kanthal A ribbon heating unit. The bottom of the tubes were closed except for a platinum - platinum/13-percent-rhodium thermocouple exposed in one of the tubes adjacent to the specimen. In this test setup the air was also essentially still.

The specimens were automatically raised and lowered by pneumatic cylinders controlled by reset timers, as shown in figure 3. As the samples were raised, they were individually shielded to prevent cross-spall and the six cups automatically slid under the samples to catch the oxide which spalled on cooling. This sequence occurred in

roughly 10 seconds. The amount of cross-spall is well under 1 percent because the sample is almost completely enclosed as it cools and the spall for each sample was trapped in its own metal foil cup. The samples were removed and weighed once a day to generate a ΔW-against-time curve. The spall was collected over the whole test and thus represents an integrated composition.

Postoxidation Procedure

After each of the two types of tests, the condition of the sample and its degree of spalling was noted. The retained oxide on the sample and its spall were analyzed by X-ray diffraction (XRD). The samples were then sectioned horizontally across their centers and mounted to determine their thickness metallographically. The thickness change is the difference between the initial preexposure measurement by a micrometer at the center of a sample and the postexposure metallographic thickness. Here the cross section was photographed at either 35X, 50X, or 100X. A millimeter filar grid at the same magnification was also photographed and used in measuring the photomicrograph to correct for optical distortion. Because of variability in the sample thickness and errors in measurement, it is estimated that the thickness change was determined to within ± 0.015 millimeter.

RESULTS

Isothermal and Cyclic Data

After the isothermal tests, the spall caught by the individual beakers on final cooldown and the total accumulated spall from each spall cup from the cyclic tests were collected (where available) for each alloy. The amount of total spall collected for each sample was rated from no visible (negligible) spall to massive spall.

The alloys were classified according to the weight of spall collected divided by the geometrical sample area in mg/cm^2 as follows:

Negligible spall	0 to 0.25
Light spall	0.25 to 2.00
Moderate spall	2 to 10
Heavy spall	10 to 50
Massive spall	>50

These spall descriptions are listed in table II for isothermal and in table III for cyclic runs, along with the X-ray diffraction results on both the retained surface oxides

and the spalled oxides. The spalls collected after cooling from the isothermally run samples were also rated although they do not relate directly to the isothermal process. If the surface X-ray pattern indicated the underlying metal solid solution was detected, this was also noted. Detection of the solid solution implied that the oxide was not thick enough to completely attenuate the X-ray beam. The phases detected are listed in tables II and III along with their diffraction intensities. When a spinel was detected, its lattice parameter a_o is listed as well.

Table IV lists the 100-hour ΔW values for both the isothermal and cyclic tests. The isothermal value represents the final weight at temperature after 100 hours of exposure prior to any spalling on cooling. For the cyclic data this 100-hour sample weight represents the final weight after cooling from the one-hundredth 1-hour heating cycle.

Many of the continuous isothermal curves plotted as ΔW against time were approximately parabolic. For the sake of brevity, these are not shown. (Specific isothermal curves are discussed in more detail in the section DISCUSSION OF RESULTS.) The reproducibility of the isothermal tests is estimated to be about 20 percent.

For the cyclic data, most of the ΔW values were derived from duplicate samples in different runs and agree to within 10 percent - see appendix A. Chromel P, Hastelloy-C-276, and Multimet had excessive weight loss relative to their initial thickness. These materials, as well as TD-NiCr and TD-NiCrFe, were not run as duplicates. The 100-hour data for the first three materials were extrapolated from shorter time, single-run data. The 100-hour ΔW values for both the isothermal and cyclic exposures are used herein to calculate an approximate sample thickness change.

The 25 individual alloy plots of ΔW against time for each alloy in the cyclic oxidation tests are shown in figure 4 with the data from separate runs indicated by two sets of symbols. The time-scale abscissa on all the plots is the same, 0 to 100 hours. The ordinates, however, are adjusted based on the maximum and minimum specific weight change values in mg/cm^2 observed for each alloy. As previously mentioned, three of the alloys plotted in figure 4 lost weight so rapidly (massive spall: Chromel P, Hastelloy-C-276, and Multimet) that they were not run for the full 100 hours. For Hastelloy-C-276 and Multimet this excessive weight loss was due in part to volatile MoO_3 formation as detected by the heavy deposit of that oxide on the hanger wire and, more importantly, to severe spalling. Most of these severe spalling curves resemble paralinear oxidation curves.

The thickness changes are also listed on table IV and plotted as bar graphs in figure 5. In many cases there are two values noted: one for general penetration and one for measured thickness change plus grain boundary penetration (or possibly internal oxidation). The grain boundary penetration values are designated in table IV and figure 5 by the letter G next to the value.

Also included in table IV is a designation of the smoothness or convolution of the

oxide/metal interface as determined from metallography at 250X. This description is used in the discussion of scale adherence in a later section.

Mass-Balance Approach

High-temperature cyclic oxidation can involve three nearly simultaneous processes - scale growth and scale component vaporization at temperature and scale spalling as the sample cools or is heated to test temperature[1]. The mass balance equation after any cycle can be written as follows:

$$\Delta W = W_r \frac{1}{b_r} - W_v \frac{a_v}{b_v} - W_s \frac{a_s}{b_s} \qquad (1)$$

ΔW	net sample specific weight change, as defined previously, mg/cm^2
W_r	specific weight of retained oxide, mg/cm^2
W_v	specific weight of vaporized oxide, mg/cm^2
W_s	specific weight of spalled oxide, mg/cm^2
a	ratio of atomic weights of metal to oxygen in oxide
b	ratio of molecular weight of oxide to oxygen in oxide

The subscripts relate to retained, vaporized, or spalled oxides.

Conventional isothermal gravimetric tests measure only the W_r term (in slightly different form). If oxide vaporization is occurring, the W_v term is implicitly involved. These are just special cases of equation (1).

From equation (1) the total amount of metal W_m per unit area converted to oxide can be calculated.

$$W_m = W_r \frac{a_r}{b_r} + W_v \frac{a_v}{b_v} + W_s \frac{a_s}{b_s} \qquad (2)$$

[1]Scale spalling at temperature is negligible.

where $W_r(a_r/b_r)$, $W_v(a_v/b_v)$, and $W_s(a_s/b_s)$ can be defined as W_{mr}, W_{mv}, W_{ms}, respectively. These are the amount of metal per square centimeter in the retained oxide, vaporized oxide, and spalled oxide, respectively. So equation (2) can be written as

$$W_m = W_{mr} + W_{mv} + W_{ms} \tag{3}$$

The metal consumed in mg/cm^2 can then be converted to change in thickness Δt in micrometers for <u>one</u> side of the sample by

$$\Delta t = kW_m/\rho_{met} \tag{4}$$

where ρ_{met} is the weighted average density in g/cm^3 as estimated from X-ray diffraction of all the metallic elements converted to oxide and k is a conversion factor used, in this case, to convert from W_m in mg/cm^2 to micrometers for Δt. This is an effective thickness change in that it is assumed to be uniform. There is no obvious way of calculating local depth or extent of grain boundary oxidation.

Equation (1) should provide a method for determining the amount of oxide formed by any of the three processes since it depends on ΔW, the net sample weight change which can be determined directly by weighing the sample, and on some method of determining any two of the three weights W_r, W_v, and W_s. The various stoichiometric factors for each oxide are derived from X-ray diffraction data. These factors can be complicated if mixed oxides are present, but since ratios are involved their values do not vary dramatically. The W_v values can be determined if the vaporization rate k_v for Cr_2O_3 or other vaporizing oxides, can be determined. The major uncertainty in the analysis is expected to be determining the specific weight of the spalled oxide W_s or the specific weight of the retained oxide W_r.

DISCUSSION OF RESULTS

Isothermal Oxidation

Classically, isothermal oxidation analysis assumes the process is diffusion controlled. Thus, the parabolic scaling constant k_p has been the most important derived parameter. Here the oxidation process in terms of oxygen weight gain is

$$\Delta W = k_p^{1/2} t^{1/2}$$

where ΔW is the specific sample weight change at any time t. This k_p value is usually computed from the slope of $(\Delta W)^2$-against-time plots based on the final point (e.g., the 100-hour ΔW value) and earlier steady-state points. If, as is expected, vaporization of Cr_2O_3 as CrO_3 might be a factor, the preceding equation can be modified in the approximate form:

$$\Delta W = k_p^{1/2} t^{1/2} - k_v t$$

where k_v is the rate of Cr_2O_3 loss as CrO_3. This is the so-called paralinear approximation of a plot of a sample specific weight change against time. It is characterized by a curve first reaching a maximum followed by a nearly linear drop into the negative weight change region. This drop is caused by the oxide approaching a limiting thickness. When this correction is used later in the report, the more exact form (refs. 4 and 5) is used because it allows direct determination of the total amount of metal converted to oxide, along with the degree of buildup of a limiting oxide thickness.

For isothermal oxidation the alloys examined in this study can be placed in four main categories based mainly on XRD and isothermal weight change data as follows:

(1) Category I - NiO control: TD-Ni; first stage, Chromel P(10 Cr)

(2) Category II - Cr_2O_3/chromite spinel control: first stage, IN-702 (16 Cr); second stage, Chromel P; all other high Cr, Ni, Fe, and Co alloys (>16 Cr)

(3) Category III - αAl_2O_3/aluminate spinel control: second stage, IN-702(3 Al); all FeCrAl alloys and TD-NiCrAlY(16 Cr, 3.5 Al)

(4) Category IV - ThO_2-blocked Cr_2O_3 control: TD-NiCr and TD-NiCrFe

The alloys are listed according to these classifications in table V.

The alloys in categories III and IV and in the lower range of category II can be considered to have good resistance in low-velocity isothermal oxygen. For categories I and III, where cyclic spalling was negligible, the cyclic data were used to derive the isothermal rate constant k_p based on the slope of ΔW-against-time plots. These constants (including in some cases a second-stage parabolic constant) are listed in table V. Categories II and IV, on the other hand, are basically Cr_2O_3-forming alloys. And therefore it is thought that vaporization of CrO_3 makes the specific weight-against-time change paralinear. For TD-NiCr and TD-NiCrFe this is obvious since their ΔW-against-time curves attain negative slopes in well under 100 hours. The category II alloys were thought to occur early in the paralinear weight change process. Their values were well before the maximum but still tended to flatten out somewhat so as not to be strictly parabolic.

In applying this paralinear approach to the 15 or so category II alloys in this report, the simplest technique was to pick the 100-hour isothermal ΔW value and an extrapolated k_v of 0.0081 for Cr_2O_3 vaporization as CrO_3 from similar alloys (ref. 6)[2] and then to generate the complete isothermal paralinear curve. Thus, 0.55 milligram of Cr is vaporized every 100 hours per square centimeter of area. Isothermal paralinear curves were generated, as described in reference 5, and the fit was quite good compared with the experimental isothermal curve in most cases. This type of analysis was performed on 15 alloys (including two duplicate runs) to generate 17 ΔW-against-time plots. In 13 cases the fit was very good, in one case it was good, and in three cases it was fair. Typical experimental and derived curves are shown in figure 6. Based on this analysis, the hypothesis that Cr_2O_3 vaporization at 1150° for 100 hours could alter the usual ΔW-against-time curve was accepted. This result was also suggested by Lewis (ref. 6). Also for all the alloys tested, a k_v of 0.0081 mg/cm^2/hr was close enough to the vaporization rate of Cr_2O_3 under these test conditions (in spite of the compositional differences in alloys) to generate a valid weight change curve. Table V also gives the predicted times when the paralinear specific weight change curve will reach a maximum and when it will return and cross zero weight change. The maximum ΔW is predicted as well.

Comparable values listed in table V were derived for TD-NiCr and TD-NiCrFe. Values for k_p and k_v were determined from the 100-hour ΔW values (using the cyclic test data since spalling was negligible) and from the crossover time when ΔW is again zero. For the ThO_2-blocked Cr_2O_2-forming alloys, these k_p and k_v values are less accurate since k_p is apparently dropping until the downslope in the ΔW-against-time

[2]The Lewis' data (ref. 6) for long-time isothermal oxidation at 1200° C (>1000 hr) were used to derive a k_v for Ni-20Cr-3Fe-0.4Si by paralinear analysis (ref. 5). This value was back extrapolated to 1150° C along the slope of a bulk Cr_2O_3 vaporization curve derived by Hagel (ref. 7).

curve is reached. This steady-state k_p value, may be a factor of 5 or 10 lower than the initial value.

For the alloys for which this paralinear analysis holds, the chromium compositions are greater than 16 percent Cr and aluminum compositions are less than 4 percent.

The oxidation data in table V are summarized in figure 7 for the four scale-forming classes. On the plot are two bands of k_p values derived by Goward (ref. 8) as a function of temperature. The lowest band represents the oxidation of an alloy with αAl_2O_3 (with dissolved Cr^{3+} cations) as the rate controlling scale, and the upper band represents Cr_2O_3-controlled oxidation. Also shown is the broad band of k_p as a function of inverse temperature as given by Evans[3] (ref. 9). This band represents the spread of k_p for Ni-Cr heater alloys and other alloys for which it is claimed Cr_2O_3 formation is critical. This band is considerably lower than Goward's band for Cr_2O_3 control. An NiO-forming band is also plotted for 1150° C which falls in the range expected from a recent oxidation study of nickel (ref. 10). In general, the rate constants derived from this investigation fall in the anticipated regions on the plot if Evans' band is used for the alloys classed in this study as Cr_2O_3/chromite spinel formers.

Also plotted are the very low rate constants for the Cr_2O_3-forming TD alloys: TD-NiCr and TD-NiCrFe. They are effectively lower than the $\alpha Al_2O_3(Cr^{3+})$-forming range apparently because of ThO_2.

The alloys forming Cr_2O_3/chromite spinel show the most complex and wide-ranging behavior in isothermal oxidation of the four classes presented herein. Presumably in this type of alloy the base metal oxide (NiO, FeO, and CoO, or in general metal monoxides (MeO)) and the Cr_2O_3 compete for nucleation in the early stages of oxidation. Finally, if the Cr content in the alloy is high enough, it will form a continuous layer of Cr_2O_3. The MeO will form over the growing Cr_2O_3 layer, and it will also grow by the migration of Me cations through the Cr_2O_3 where the MeO continues to form. The Cr_2O_3 and MeO tend to react to form the $MeCr_2O_4$ spinel between them. This reaction is usually fast enough so MeO is not observed by XRD. The question remains as to what is controlling the overall rate of oxidation. It has been shown that the spinel layer can form a continuous overlayer on WI-52 alloy (ref. 11), although this is difficult to observe metallographically. Because of the paralinear kinetics observed, isothermal oxidation still appears to be partly a diffusion-controlled process. This could account for the wide range of k_p values, which can vary by a factor of nearly 25, reported in the literature for so-called Cr_2O_3-forming alloys like 80Ni-20Cr. This wide range of values is not caused by lack of reproducibility, as can be seen from dupli-

[3]The values plotted by Evans were not corrected for Cr_2O_3 vaporization but are for the most part first-stage parabolic scaling constants, which tend to be higher than second-stage constants. Therefore, they would be more in line with k_p's corrected for vaporization.

cate tests, but by real differences between alloys of differing compositions that could change the relation of the three scale-forming processes. It is not clear if the spinel formed actually raises or lowers the effective rate of oxidation (i.e., metal consumption) as compared with the Cr_2O_3 or whether it gives an overall thicker or thinner scale. It does tend to spall drastically on cooling, however, leaving Cr_2O_3 and patches of spinel behind as the retained oxide. This spalling could be caused by the presumed mismatch in thermal expansion coefficients of the spinel and Cr_2O_3 as well as by an overall oxide thickness effect. The spinel/MeO overlayer would also tend to lower the vaporization rate for Cr_2O_3 dissolved in MeO since the Cr would have a lower concentration on the outer surface than in pure Cr_2O_3. This could explain the difference in k_v values (0.012 as compared with 0.0081) listed in table V for the two Cr_2O_3-forming alloys derived from the paralinear analysis previously described.

It is difficult to correlate the composition of the Cr_2O_3/chromite-spinel-forming alloys with their isothermal rate constants. Multiple linear regression analysis (without interactions) of k_p as a function of Fe, Cr, Al, Si, Mn, and C showed no significant correlation.

The αAl_2O_3/aluminate-spinel-forming alloys apparently behave as follows: In simple binary alloys of Ni-Al, Fe-Al, or Co-Al, well over 10 percent aluminum is needed to form $\alpha\, Al_2O_3$. At lower aluminum concentrations, MeO or other oxides are formed (ref. 12). It was observed in reference 12 that when chromium (10 to 15 percent or higher) is alloyed with Ni-Al or Fe-Al systems, the aluminum level required for Al_2O_3 formation is only 3 to 5 percent. The $\alpha\, Al_2O_3$ contained dissolved Cr^{3+} cations, however. In this study, aluminate spinels (a_o = 0.81 to 0.82 nm (8.10 to 8.20 Å)) were occasionally detected along with αAl_2O_3. This general type is classed as an αAl_2O_3/aluminate spinel former.

Here the αAl_2O_3/aluminate spinel was even more oxidation resistant than the best Cr_2O_3/chromite-spinel-forming alloy. The sample oxidation curves also tend to flatten out somewhat just as do the Cr_2O_3/spinel-forming alloys. This flattening was interpreted as the k_{p2} portion of the curve, but also it could be consistent with CrO_3 vaporization at very low rates from the dissolved chromium in the αAl_2O_3.

Cyclic Oxidation

A good comparison between cyclic and isothermal oxidation behavior is in the actual metal thickness change at the end of a test. The problem in measuring thickness change is discussed in appendix B. It is assumed that the more the alloying or base metal elements are converted to the oxide and spall (along with any oxide vaporization), the greater the total metal consumption and thickness change. Thus the samples with a greater tendency to spall (tables II and III) and greater weight change (table IV) will have

the greatest thickness change for the samples tested cyclically. An examination of figure 5 shows this in general to be true. This assumes that no other metallurgical process is operating to expand or contract the metal to a significant degree - which is usually the case.

As developed in the literature (refs. 13 to 23) there are four main factors generally associated with improved spalling resistance in cyclic oxidation exposure. In this investigation they would apply as follows: (1) the thinner the oxide formed, the less the degree of spalling; (2) the scale should be mainly the sesquioxide Cr_2O_3 (or αAl_2O_3) (the less NiO or comparable monoxide and/or spinel formed with the sesquioxide, the less the degree of spalling); (3) if possible, the scale should be keyed or pegged onto the metal; and (4) there should be good matching of the oxide lattice to the substrate (e.g., NiO on TD-Ni). The third factor is still not well understood but is usually based on internal oxidation of various reactive alloying additions, including silicon. Internal oxidation of these additions supposedly leads to an irregular, or convoluted, surface and/or intimate contact between the internally formed oxides and the external scale[4] (ref. 20). Apparently, the Al_2O_3-forming alloys also depend on these same four factors (refs. 22 to 24).

Recent work on αAl_2O_3/aluminate-spinel-forming alloys indicate that the aluminate spinel is not associated with the onset of spalling. Rather it is the chromium which tends to enter the spinel lattice at later times and raise the a_o so it is effectively a chromite spinel close to or greater than 0.825 nanometer (8.25 Å). Thus, in both category II and III scale-forming types, eventual chromite spinel formation is associated with severe spalling.

With the exception of TD-Ni, which forms NiO on a nickel matrix, the alloys with the lowest isothermal rate constants (i.e., which lead to the thinnest scales) generally spall the least. The major exception was the Cr_2O_3-forming HA-188, which has a rate constant just above the range of αAl_2O_3/aluminate spinel alloys but which spalled heavily[5] in cyclic oxidation. This may be the nature of cobalt-base alloys, since the only two tested in this study spalled severely. Generally, the Cr_2O_3-forming alloys with the most complex compositions spall the most. The cause appears to be the greater tendency for spinel formation. A comparison of XRD results for both continuous and cyclic data shows that the alloys which tend to spall the most upon cyclic oxidation are those that in isothermal oxidation tend to form NiO and then spinels along with the Cr_2O_3. And when these alloys were tested cyclically the degree of NiO and/or spinel formation was enhanced further. This in turn accelerated spalling.

---

[4]This appears to be a question of degree. Too much convolution could increase the effective surface area drastically or lead to severe grain boundary oxidation.

[5]Later cyclic tests on HA-188 with a lightly etched surface showed the spalling to be significantly less. This difference is currently being investigated.

In an XRD and X-ray fluorescence analysis of cyclically oxidized samples (refs. 16 and 17), Grisaffe and Lowell showed the association of spinel formation with spalling (ref. 18) for some of the same alloys tested in the present study.

The one exception to the preceding generalizations could be IN-702. If we examine both the ΔW-against-time plots and the X-ray results for both the continuous and cyclic tests of IN-702, it appears the initial buildup is caused by Cr_2O_3 formation, as was discussed in the isothermal oxidation section. IN-702 then starts to behave like an alloy which forms αAl_2O_3/aluminate spinel. If the alloy is cycled, apparently this latter tendency is accentuated and the weight change curve levels off after the initial spalling (see fig. 4). This result is verified by the spall of the cyclic test, which was mainly Cr_2O_3 and a chromite spinel (a_o = 0.835 nm (8.35 Å)). X-ray diffraction of the retained oxide detected αAl_2O_3 and an aluminate spinel (a_o = 0.815 nm (8.15 Å)). The presence of this latter spinel seems indistinguishable in overall oxidation and spalling resistance from an αAl_2O_3 scale with chromia in solution (ref. 23).

The trend in recent years has been to add as much as 1 percent of the reactive metals, in addition to the silicon which may be present in conventional oxidation-resistant alloys, to these alloys to improve further their overall oxidation resistance. The alloys so modified in this investigation were TD-NiCrAlY with yttrium and thorium as ThO_2, TD-NiCr and TD-NiCrFe with thorium as ThO_2, GE-1541 and GE-2541 with yttrium, and HA-188 with lanthanum. The reactive refractory metal niobium was added to DH-242. These reactive metals not only in some cases are supposed to "key" the oxide, but also the Group IIIA metals in particular have been shown to lower the oxidation rate and to stabilize either Cr_2O_3 (see isothermal HA-188) or αAl_2O_3 at the expense of spinel formation and further lower cation diffusion. This may be the real role of silicon and yttrium in Cr_2O_3-forming alloys - to stabilize Cr_2O_3 (refs. 25 and 26). Besides keying, sesquioxide stabilization should lead to thinner oxides and hence less spalling (refs. 13 and 23). The lattice matching between oxide and metal improves also (ref. 15). In αAl_2O_3/aluminate-spinel-forming alloys, yttrium confers no obvious additional benefit to TD-NiCrAlY since the ThO_2 appears to be the critical alloy addition. The oxidation resistance of GE-1541 and GE-2541, which contain yttrium, is slightly poorer than that of HOS-875. The role of yttrium in category III scale-forming alloys is undergoing further investigation. Yttrium is thought to be redundant in thoria dispersed (TD) alloys.

Of the four critical factors to minimize spalling, it seems factors (1) and (2) mainly resolve into keeping the oxide thin. Factor (3) keying may in reality be a thin-scale effect also. If a spinel is present, it will probably be thicker than a sesquioxide and hence more prone to spall. Indeed there may be more of an advantage to an alloy like TD-NiCr since it was observed that Cr_2O_3 vaporization keeps the oxide even thinner than the αAl_2O_3 formers (ref. 27). This alloy does not spall until spinels are formed

at very long times by chromium depletion caused by Cr_2O_3 vaporization. An additional question arises in considering the cobalt-base alloy HA-188. It has a very low isothermal rate of scale buildup with lanthanum present and should remain thin and keyed. It does spall badly, however, in these cyclic tests.

To test the hypothesis of a convoluted metal/oxide surface conferring spalling resistance, an attempt was made to classify the oxide/metal surface as to whether it was convoluted or fairly smooth. This classification was done by examining 250X photomicrographs of the cyclically tested samples. Two typical examples from each class are shown in figure 8. The Hastelloy X has a very irregular oxide along with what appears to be some internal oxidation. The HOS-875 has a very smooth, clean metal/oxide interface. All the available cyclic samples were placed in either the convoluted or smooth category as designated in table IV. Based on this classification the best and worst of the alloys fall into both groups. Alloys containing the reactive metals previously discussed also fall into both groups. Thus, there is no apparent correlation between the degree of convolution of the oxide/metal interface and its spall resistance. Perhaps a similar classification at higher magnification would be more informative.

In summary, the most critical factor in minimizing scale spalling found in this study is to keep the surface oxide as thin as possible consistent with a low rate of metal consumption. This is most obviously done by forming exclusively a sesquioxide, Cr_2O_3 or αAl_2O_3. The low rate of formation of these sesquioxides, in turn, keeps the rate of scale buildup low. The spinels formed by nickel, cobalt, or iron cation migration through the sesquioxide tend to produce spalling by the formation of a thicker oxide with a greater tendency to spall and/or by the probable mismatch of expansion coefficients at the sesquioxide/spinel interface. Aluminate spinels, however, appear in this and related investigations to behave similarly to αAl_2O_3 (ref. 23). The eventual breakdown of an αAl_2O_3/aluminate spinel scale is thought to be caused by chromite spinel formation resulting from the high chromium levels in the alloys. A thin layer of base metal monoxide could be present over the spinel as well.

From this investigation there is no evidence that scale "keying" is a real effect. Recent work by Tien and Pettit (ref. 28) indicates that scandium or yttrium as dispersed oxides or any finely dispersed phase such as Al_2O_3, ThO_2, or possibly SiO_2 improve scale adherence by minimizing void formation at the oxide/substrate interface. This could explain the role of ThO_2 in the thoriated alloys and eliminate the need for Y in such alloys.

Mass-Balance Approach

As is outlined in the section RESULTS, the mass-balance approach involved the following critical equations:

$$\Delta W = W_r \frac{1}{b_r} - W_v \frac{a_v}{b_v} - W_s \frac{a_s}{b_s} \tag{1}$$

and

$$W_m = W_r \frac{a_r}{b_r} + W_v \frac{a_v}{b_v} + W_s \frac{a_s}{b_s} \tag{2}$$

The cyclic test apparatuses described in this report were designed to measure directly the specific sample weight ΔW and particularly the specific sample spall weight W_s.

It was thought for the type of spall catchers shown in figure 3 that close to 100 percent of the spall could be collected. However, an analysis of the test results based on metallographic estimates of W_r, as well as on special runs with samples in enclosed quartz containers, shows in figure 9 that at best about 80 percent of the spall can be collected. With samples that spall very little, only about 10 percent can be collected. Thus, most of the spall is lost, probably within 10 seconds of leaving the hot zone and particularly for the most resistant alloys. This "lost spall" problem seems endemic to cyclic tests. For this reason, either special modification of cyclic test apparatus or calibration runs of the type shown in figure 9 would be necessary to determine W_s for use in equation (1). Thus, the uncorrected W_s value is useful only as a rough rating guide unless spall collection for the apparatus can be calibrated. This suggests that equal emphasis should be placed on determining W_r, the amount of retained oxide. In a sense this situation is fortuitous since in high-velocity gas burner rig tests (designed to simulate aircraft engine environments), for example, W_s cannot be estimated anyway. If equations (1) and (2) are added and the terms are rearranged, W_m can be found directly, independent of W_v and W_s:

$$W_m = W_r\left(\frac{1}{b_r} + \frac{a_r}{b_r}\right) - \Delta W$$

or

$$^{6}W_m = W_r - \Delta W \qquad (5)$$

where ΔW can be determined by direct weighing and the term in parentheses is equal to unity since $b_r = a_r + 1$. Thus, in running a meaningful cyclic oxidation test, the key can be measuring W_r. For this investigation W_r was determined by metallography. But if some nondestructive technique could be developed (e. g., the beta-ray reflection technique currently being examined), this could be of considerable importance in establishing an oxidation rating parameter for tests as different as conventional isothermal gravimetric oxidation tests and burner rig tests. A flow diagram outlining the mass-balance approach is shown in figure 10.

Equation (5) was used to determine W_m for the cyclic tests. This W_m value for the isothermal runs could be determined directly either from straight parabolic oxidation, as with TD-Ni or HOS-875, or from the paralinear analysis when Cr_2O_3 vaporization was a factor. On this basis, W_r could be determined directly for the isothermal runs. For the cyclic tests in this study W_r was derived by comparing the amount of retained oxide determined by metallography with that from the comparable isothermal test. This oxide thickness ratio (cyclic/isothermal) was used to multiply the W_r isothermal value to give the cyclic W_r value. These ratios are listed in table VI and range from 1 for an alloy like Tophet 30 to 3 for Chromel C. The two appropriate sets of comparative photomicrographs for these alloys are shown in figure 11. This is a first approximation; more precise measurements of W_r are needed.

The chief advantage of the mass-balance approach (fig. 10) is that measurements can be made intermittently on the sample without destroying it. Since the W_m value derived is a direct measurement of the total oxidation process (i. e., total metal converted to oxide), it would be of fundamental interest to follow it as a function of time (i. e., cycles), temperature, and so forth. Oxidation kinetics of a cyclic oxidation process which

[6]This is the same net result as that developed for paralinear analysis (ref. 5).

includes scale growth, scale spalling, and vaporization have not lent themselves to even simple mathematical modeling. It is hoped the W_m parameter will be useful in this regard. Also W_m, rather than effective Δt or the actually measured Δt, may ultimately prove to be the best rating parameter to compare alloys short of a mechanical test. This could be especially true for cases involving metal depletion, where the Δt values can be ambiguous (ref. 24).

As shown in figure 10 the key to the mass-balance approach is in determining W_r, which then leads directly to W_m. In this study, because there was some question in determining the true spall weight, the actual approach used was the metallographic ratio of cyclic to isothermal sample scale thickness previously described. This approach was used to verify the method. Future tests will concentrate on nondestructive evaluation techniques (NDE) and spall collector techniques which do not require destruction of exposed samples.

The W_m results from table VI allow the alloys to be rated quantitatively. Equation (4) can be used to convert this W_m value to an "effective" thickness change if we assume that the approximate average of the metal densities is converted to scale. Since these values are for attack from one side, they are compared with one-half of the total measured thickness-change values discussed earlier. These comparisons are listed in table VI.

The derived thickness-change values from one side are plotted against the comparable measured values for both the isothermally and cyclically tested samples on a log-log plot in figure 12. The perfect fit line (45° line) is shown as well, and the estimates appear good. If the derived values are multiplied by 3 (indicated by the dashed line), the extent of grain boundary oxidation can also be estimated. Virtually all the samples fall within this limit, particularly the cyclically tested ones. The three isothermal values well outside the estimate in the upper range probably result from overestimating the degree of grain boundary oxidation (appendix B). This shows a certain ambiguity in measuring the degree of grain boundary attack and indicates W_m might be a more objective criterion. It also points out the possible advantage of a postoxidation tensile test which directly indicates the remaining effective area of unattacked alloy. As mentioned earlier a measured Δt ordinarily does not include depletion (e.g., Cr diffusion out of Ni-Cr alloys to form Cr_2O_3) unless a phase change occurs and is detected by etching or unless an electron microprobe trace delineates the depletion zone. The W_m estimate (and therefore the derived Δt_{W_m}) from the mass-balance analysis would include this effect, which may be an additional advantage of the W_m approach. We are assuming that alloy depletion is detrimental to the service life of the alloy. In virtually all cases, multiplying the Δt_{W_m} estimate by three would include the maximum grain boundary penetration and would be a reasonable maximum attack limit for design purposes.

Based on these results, the alloys, both isothermal and cyclic, can be ranked on a common basis. Summarized data and rankings are listed in table VII. The alloy rankings are plotted in figure 13 schematically as bar graphs indicating the effective amount of attack based on the mass-balance derivation. They are placed in five arbitrary oxidation resistance categories from excellent to catastrophic based on the amount of area loss due to thickness change (and therefore assumed loss in effective tensile strength of a 0.254-mm (0.010-in.) thick tensile sample occurring in the total oxidation process). The alloys rated excellent are those that have from 95 to 100 percent of the specimen area left, good - 90 to 95 percent, fair - 75 to 90 percent, poor - 50 to 75 percent, and catastrophic - less than 50 percent of the specimen area remaining. The solid bar indicates cyclic attack, while the open bar indicates isothermal attack. When only a solid bar is shown with an asterisk, both types of attack are considered equal. The alloys are grouped in ascending order of cyclic attack from left to right on the figure.

Figure 13 shows that the cyclic oxidation behavior of alloys that were isothermally classed as NiO, ThO_2-blocked Cr_2O_3, or αAl_2O_3/aluminate spinel scale control formers does not differ drastically from their isothermal behavior. The behavior of Cr_2O_3/chromite-spinel-forming alloys, on the other hand, can vary widely. For the simpler high-chromium-content alloys such as Tophet 30 and DH-242, the cyclic rate of attack is only slightly greater than the isothermal. For the more complex alloys such as HA-188 and Hastelloy-C-276, the cyclic attack is much more severe. This difference results from the strong tendency of this type of alloy to form spinels because of an extremely sensitive critical chromium level.

What this means in cyclic oxidation is that increasingly complex Cr_2O_3-forming alloys must have very high chromium levels to avoid chromite spinel formation. However, at temperatures above about 1100° C, even such high chromium levels would be rapidly depleted near the surface by vaporization. This depletion would allow spinels to form and would produce severe spalling. Unless the Cr_2O_3 vaporization problem can somehow be eliminated (preferably by alloying), αAl_2O_3/aluminate-spinel-forming alloys appear to be the only alternative for cyclic applications primarily above 1100° C. Future oxidation work will probably focus on the characteristics of αAl_2O_3-forming alloys.

SUMMARY OF RESULTS

The isothermal and cyclic (with 1-hour heating cycles) oxidation behavior of 25 nickel-, cobalt-, and iron-base sheet alloys in air at 1150° C for 100 hours was studied. The salient results can be summarized as follows:

1. In isothermal oxidation, when steady state is reached, the alloys tested fall into four general classes:

a. Category I - NiO control (parabolic scaling constant, k_p, >1.0$(mg/cm^2)^2/hr$): for example, TD-Ni and Chromel P (first stage)

b. Category II - Cr_2O_3/chromite spinel control (k_p, 0.036 to 0.377 $(mg/cm^2)^2/hr$): for example, HA-188, DH-242, and IN-601

c. Category III - αAl_2O_3/aluminate spinel control (k_p, 0.0096 to 0.025 $(mg/cm^2)^2/hr$): for example, TD-NiCrAlY, HOS-875, and IN-702 (second stage)

d. Category IV - ThO_2-blocked Cr_2O_3 control (limiting k_p, ~ 0.0065 $(mg/cm^2)^2/hr$): for example, TD-NiCr and TD-NiCrFe

2. In general, Cr_2O_3/chromite spinel formation is favored if more than 16 percent chromium is present in the alloy, unless more than 4 percent aluminum is also present. In the latter case α Al_2O_3/aluminate spinel control is favored.

3. In isothermal oxidation at 1150° C, both the Cr_2O_3/chromite spinel and the ThO_2-blocked Cr_2O_3-forming alloys can have scaling rate constants low enough compared to the apparent $Cr_2O_3(s) + 3/2\ O_2(g) \rightarrow 2CrO_3(g)$ vaporization rates that paralinear kinetics are observed in the plots of specific weight change against time. Therefore, the derived k_p values for the Cr_2O_3-forming alloys were corrected for Cr_2O_3 vaporization by paralinear analysis.

4. The cyclic oxidation behavior of alloys that isothermally form NiO, Cr_2O_3 (ThO_2 blocked), and αAl_2O_3/aluminate spinel does not differ significantly from their respective isothermal behavior. The cyclic oxidation behavior of alloys that isothermally form Cr_2O_3/chromite spinel, on the other hand, can degrade severely in cyclic testing. This tendency toward spinel formation and spalling in the Cr_2O_3-forming alloys increases with the complexity of the alloys and decreasing chromium content in the alloy.

5. By using a mass-balance approach, an oxidation attack parameter based on the TOTAL specific metal converted to oxide W_m can be derived from gravimetric measurements whether or not this oxide is retained, spalls, or is vaporized. This value can be converted to an effective sample thickness change which is in good agreement with metallographically measured thickness changes.

6. Other factors which appear to contribute to good scale adherence, which minimizes the tendency to spall on thermal cycling, are thin oxides and the addition of small amounts of rare earths and reactive elements. Thin oxides (i.e., a low isothermal k_p) form, for example, on TD-NiCr (further enhanced by Cr_2O_3 vaporization). The reason for the beneficial effect of adding rare earths and reactive elements is not firmly established; but small amounts of silicon are important in nickel-chromium heater alloys, while lanthanum, niobium, and thorium have also proven beneficial in small amounts in various alloys. In this study yttrium additions particularly in thoria-dispersed alloys offered no apparent advantage, and highly convoluted metal/

oxide interfaces appeared to have no consistently beneficial effect on scale adherence through oxide "keying."

CONCLUDING REMARKS

All Cr_2O_3-forming alloys are highly susceptible to scale vaporization at high temperatures. Attempts to significantly lower this vaporization rate by alloying has not been successful. This vaporization in turn leads to chromium loss and severe spalling on cycling as the chromium level is lowered and increased chromite spinel formation occurs. It is recommended that nickel-, iron-, and cobalt-base alloys for service near 1100° C contain aluminum, leading to $\alpha\, Al_2O_3$/aluminate spinel formation. This is the current trend in cast nickel-base $\gamma + \gamma'$ aircraft gas turbine alloys. The aluminum originally added for γ' formation also contributes to $\alpha\, Al_2O_3$ formation. The oxidation properties of such alloys have been little explored, but some chromium is necessary to allow the $\alpha\, Al_2O_3$ to form exclusively at lower practical aluminum contents. In the commercial $\alpha\, Al_2O_3$/aluminate-spinel-forming alloys the optimum quantities of chromium and aluminum have not been determined for long-time cyclic oxidation resistance except for certain FeCrAl alloys. Small additions of reactive metals and/or silicon have not been explored vis-a-vis the total chemistry of the alloy and its various properties. The role of yttrium in particular is uncertain and should be investigated further.

It seems the αAl_2O_3/aluminate-spinel-forming alloys eventually fail because the chromium in the alloy builds up in the scale and effectively converts the aluminate spinel to a chromite spinel which in turn spalls. Iron-base αAl_2O_3/aluminate-spinel-forming alloys, for reasons not understood, are less prone than analogous nickel-base alloys to aluminate (and hence eventual chromite) spinel formation even at chromium contents greater than 20 percent. If the reason for this difference could be understood or the chromium could be lowered or replaced by other alloying elements, a practical nickel-base alloy might be developed with the same oxidation resistance of the best of the FeCrAl alloys. Such an alloy should not require coating even at turbine temperatures approaching 1200° C.

Lewis Research Center,
National Aeronautics and Space Administration,
Cleveland, Ohio, October 18, 1973,
501-01.

APPENDIX A

REPRODUCIBILITY OF CYCLIC DATA

A general indication of cyclic test data variability can be inferred from table VIII. The table lists the net sample weight per specimen area weighed after 8, 48, and 100 hours of cycling in 1-hour cycles. The average indicated temperature for each run is also listed. The data show that, for three typical runs in three different furnaces for different alloys run in duplicate, the agreement within and between runs in generally within 10 percent. This includes alloys which gain the most weight (TD-Ni), lose a great deal of weight (L-605), or change weight only slightly (GE-1541).

APPENDIX B

THE PROBLEM OF THICKNESS MEASUREMENT

From the standpoint of rating alloys for service, the change in alloy thickness is the most direct index. It is based on the assumption that as metal is converted to oxide there is a corresponding loss in metal thickness. It is also the most limited and difficult index in that the final measurement can only be made once, after the test is completed. Usually, the scale is removed by brushing or by descaling with an electrolytic salt bath and then the sample thickness is measured (ref. 29). This approach has the advantage that if the scale can be completely removed, the same micrometer measuring technique can be used as in the pretest measurement. It has several disadvantages. Part of the metal surface may be removed along with the scale. Or often it is difficult to completely remove the scale. And if the scale is completely removed, grain boundary penetration and internal oxidation cannot be factored into the final thickness measurement. It is possible that other metallurgical processes could be operative to change dimensions as well.

Another approach is to metallographically mount the sample, section it squarely across the center, and then measure the actual remaining metal thickness observed at high magnification. This measurement can be made directly under the microscope with a filar or micrometer eyepiece. A related method is to photograph the cross section at a high magnification along with a calibrated glass slide. The thickness is then measured on the photograph and converted with the calibrated grid photographic measurement to a thickness estimate. With care, these two microscopic techniques have a variability of a few micrometers. With the variability of the thickness of material considered also, the accuracy within the field of measurement for the photographic method with an initial micrometer measurement is about 15 micrometers. This 15-micrometer band is indicated in figure 5[7]. Changes within this range could be caused by inherent variations in sheet thickness and by measurement errors, as well as by an actual thickness change. Other than using precision-ground oxidation samples, there is no apparent way around this problem.

---

[7]Seven of the duplicate cyclic samples were electrolytically descaled by the Kolene Corporation, Detroit, Michigan. XRD showed most of the oxides had been removed. Metallographic thicknesses were then measured and on the average were about 10 micrometers lower than the micrometer-measured descaled samples.

The problem involved in determining the thickness loss in the photomicrographic or microscopic methods depends on the type and degree of thickness change. Two of the most difficult alloys to evaluate are shown in figures 14 and 15. Figure 14 shows the unetched Chromel AA for both the cyclic and isothermal 100-hour tests sectioned at the center of the samples and photographed at close to 100X, each with its own grid. A set of lines drawn parallel with both surfaces represent the depth of what appears to be grain boundary oxidation. The samples were also etched and photographed at 250X, concentrating on this surface attack area. Figure 15 shows a comparable set of photomicrographs for alloy HA-188. Because of the higher initial thickness, the unetched samples of HA-188 were shot at 50X. Here a somewhat different type of grain boundary oxidation, resembling internal oxidation, is observed. Judgements like these had to be made on a good many of these alloys, which points out that thickness measurement is not an unambiguous tool in oxidation evaluation.

REFERENCES

1. Wright, I. G.: Oxidation of Iron-, Nickel-, and Cobalt-Base Alloys. Rep. MCIC-72-07, Battelle Columbus Labs. (AD-745473), June 1972.

2. Tedmon, C. S., Jr.: The Effect of Oxide Volatilization On the Oxidation Kinetics of Cr and Fe-Cr Alloys. J. Electrochem Soc., vol. 113, no. 8, Aug. 1966, pp. 766-768.

3. Giggins, C. S.; and Pettit, F. S.: The Oxidation of TD-NiC (Ni-20Cr - 2 Vol percent ThO_2) Between 900° and 1200° C. Met. Trans., vol. 2, no. 4, Apr. 1971, pp. 1071-1078.

4. Haycock, E. W.: Transitions From Parabolic to Linear Kinetics in Scaling of Metals. J. Electrochem Soc., vol. 106, no. 9, Sept. 1959, pp. 771-775.

5. Wajszel, Dominik: A Method for Calculating Paralinear Constants for the Formation of Volatile Scale. J. Electrochem Soc., vol. 110, no. 6, June 1963, pp. 504-507.

6. Lewis, H.: The Kinetics of the Oxidation Process in Nickel-Chromium-Base Alloys. Metallurgia, vol. 83, no. 495, Jan. 1971, pp. 3-8.

7. Hagel, William C.: Factors Controlling the High-Temperature Oxidation of Chromium. Trans. ASM, vol. 56, 1963, pp. 583-599.

8. Goward, G. W.: Current Research on the Surface Protection of Superalloys for Gas Turbine Engines. J. Metals, Oct. 1970, pp. 1-9.

9. Evans, E. B.: Oxidation Rate of Chromium and 80Ni-20Cr Heater Alloys. Corrosion, vol. 21, no. 8, Aug. 1965, p. 274.

10. Lowell, Carl E.; Deadmore, Daniel L.; and Grisaffe, Salvatore J.: Oxidation of TD Nickel at 1050° and 1200° C as compared to Three Grades of Nickel of Different Purity. Oxidation of Metals, vol. 4, no. 2, 1972, pp. 91-111.

11. Lowell, Carl E.; and Drell, Isadore L.: Effect of Surface Preparation on Oxidation of WI-52 at 1800° and 2000° F (1255 and 1366 K). NASA TN D-6148, 1971.

12. Giggins, C. S.; and Pettit, F. S.: Oxidation of Ni-Cr-Al Alloys Between 1000° and 1200° C. J. Electrochem Soc., vol. 118, no. 11, Nov. 1971, pp. 1782-1790.

13. Tylecote, R. F.: The Adherence of Oxide Films on Metals. J. Iron Steel Inst., vol. 195, pt. 4, Aug. 1960, pp. 380-385.

14. Wood, Graham C.: High-Temperature Oxidation of Alloys. Oxidation of Metals, vol. 2, no. 1, 1970, pp. 11-57.

15. Pfeiffer, H.: Reactions Between High-Temperature-Resistant Alloys and Gases. Reactions Between Gases and Solids. AGARD Conf. Proc., no. 52, Feb. 1970, paper 13.

16. Cole, Fred W.; Padden, James B.; and Spencer, Andrew R.: Oxidation Resistant Materials for Transpiration Cooled Gas Turbine Blades. I. Sheet Specimen Screening Tests. NASA CR-930, 1968.

17. Cole, Fred W.; Padden, James B.; and Spencer, Andrew R.: Oxidation Resistant Materials for Transpiration Cooled Gas Turbine Blades. II. Wire Specimen Tests. NASA CR-1184, 1968.

18. Grisaffe, Salvatore J.; and Lowell, Carl E.: Examination of Oxide Scales on Heat Resisting Alloys. NASA TN D-5019, 1969.

19. Gulbransen, Earl A.; and Andrew, Kenneth F.: Oxidation Studies in the Nickel-Chromium and Nickel-Chromium-Aluminum Heater Alloys. J. Electrochemical Soc., vol. 106, no. 11, Nov. 1959, pp. 941-948.

20. Lustman, B.: The Intermittent Oxidation of Some Nickel-Chromium Base Alloys. Trans. AIME, vol. 188, Aug. 1950, pp. 995-996.

21. Hickman, J. W.; and Gulbransen, E. A.: An Electron Diffraction Study of Oxide Films Formed on Nickel-Chromium Alloys. Trans. AIME, vol. 180, 1949, pp. 519-546.

22. Garlick, Ralph G.; and Lowell, Carl E.: Alloy Composition Effects on Oxidation Products of VIA, B1900, 713C, and 738X - A High Temperature Diffractometer Study, NASA TM X-2796, 1973.

23. Barrett, Charles A.; Santoro, Gilbert J.; and Lowell, Carl E.: Isothermal and Cyclic Oxidation at 1000° and 1100° C of Four Nickel-Base Alloys: NASA-TRW-VIA, B-1900, 713C and 738X. NASA TN D-7484, 1973.

24. Wukusick, C. S.: The Physical Metallurgy and Oxidation Behavior of Fe-Cr-Al-Y Alloys, Rep. GEMP-414, General Electric Co., June 1, 1966.

25. Lowell, Carl E.: Cyclic and Isothermal Oxidation Behavior at 1100° and 1200° C of Nickel - 20-Percent-Chromium, Nickel - 20-Percent-Chromium - 3-Percent-Manganese, Nickel - 20-Percent-Chromium - 3-Percent-Silicon, and Nickel - 40-Percent-Chromium Alloys. NASA TN D-7267, 1973.

26. Wood, G. C.; and Boustead, J.: The Influence of Group IIIA Metals on the Oxidation of Fe-Cr Alloys. Corrosion Sci., vol. 8, no. 9, 1968, pp. 719-723.

27. Sanders, W. A.; and Barrett, C. A.: Oxidation Screening at 1204° C (2200° F) of Candidate Alloys for the Space Shuttle Thermal Protection System. NASA TM X-67864, 1971.

28. Tien, J. K.; and Pettit, F. S.: Mechanism of Oxide Adherence on Fe-25Cr-4Ar (Y or Sc) Alloys. Met. Trans., vol. 3, no. 6, June 1972, pp. 1587-1599.

29. Lund, C. H.; and Wagner, H. J.: Oxidation of Nickel- and Cobalt-Base Superalloys. DMIC Rep. 214, Battelle Memorial Inst., Mar. 1, 1965.

TABLE I. - ALLOY CHEMICAL COMPOSITION AND INITIAL THICKNESS

Type of alloy	Alloy	Test alloy											Initial thickness, mm
		Ni	Co	Fe	Cr	Al	Si	Mn	C	Mo	W	Other	
		Content, wt.%											
$Ni-ThO_2$	TD-Ni[a]	Bal.										2.4 ThO_2	1.33
$Ni-Cr-ThO_2$	TD-NiCr[a]	Bal.			21.71							2.19 ThO_2	1.58
	TD-NiCrFe[a]	Bal.		18.14	18.79				0.02			2.5 ThO_2	1.06
Ni-Cr heater	Chromel A[b]	Bal.		0.42	19.90		1.41	0.036	0.03				2.60
	Chromel AA[b]			8.16	19.70		1.94	.16	.03				.78
	Chromel C[b]			24.10	16.60		1.27	.13	.06				.81
	Chromel P[b]			.23	9.39		.39	.002	.01				.79
	DH-241[c]			.25	19.61		1.38	2.05	.03				1.58
	DH-242[c]			1.14	19.53		1.05	.17	.04			0.92 Nb	1.59
	DH-243[c]			.60	19.43		1.38	2.01	.03				1.66
	DH-542[c]			.10	19.81		.33	.17	.08				.90
	Tophet 30[d]			.15	29.63	0.30	1.43	.01	.03				2.62
Ni-Cr-Al heater or sheet	DH-245[c]	Bal.		0.70	19.54	3.51	1.22	0.40	0.08				2.59
	IN-601[e]			13.41	23.04	1.38		.27	.04				1.54
	IN-702[e]			.50	15.44	3.08		.04	.04			0.99 Ti	2.39
	TD-NiCrAlY[a]				15.00	5.15						0.64 Y, 1.71 ThO_2	.41
Ni-base complex alloys	Hastelloy X[f]	Bal.	2.27	18.77	21.61			0.60	0.06	9.30	0.59		2.53
	Hastelloy-C-276[f]	Bal.	1.02	5.42	16.16			.47	.01	15.78	3.50	0.18 V	1.98
	IN-600[e]	Bal.	.09	7.00	15.63	0.11		.17	.05				1.62
Co-base complex alloys	L-605[f]		Bal.	1.77	20.05			1.36	0.04		14.83		0.89
	HA-188[f]	22.28	Bal.	1.78	21.50			.66	.11		14.12	0.04 La	1.60
Fe-Cr-Al heater or sheet	HOS-875[b]			Bal.	21.44	5.25		0.17	0.05				2.55
	GE-1541[g]			Bal.	14.54	4.14			.0002			0.83 Y	1.52
	GE-2541[g]			Bal.	24.55	3.83			.04			1.23 Y	2.59
Fe-base complex	Multimet[f]	20.36	19.74	Bal.	20.32			1.20	.14	3.05	2.76		2.06

[a]Fansteel Metallurgical Corp.
[b]Hoskins Manufacturing Co.
[c]Driver Harris Co.
[d]Wilbur H. Driver Co.
[e]International Nickel Co.
[f]Cabot-Stellite Corp.
[g]General Electric Co.

TABLE II. - X-RAY DIFFRACTION RESULTS AND SPALL CLASS RATING FOR ALLOY SAMPLES OXIDIZED ISOTHERMALLY AFTER EXPOSURE FOR 100 HOURS IN STILL AIR AT 1150° C

Alloys	Amount of spall[a]	Retained scale[b]									Spalled scale[b]							
		Solid solution	Cr_2O_3	αAl_2O_3	Spinel[c]	Spinel[c]	NiO	SiO_2	ThO_2	Other	Solid solution	Cr_2O_3	αAl_2O_3	Spinel[c]	Spinel[c]	NiO	SiO_2	ThO_2
TD-Ni	Negligible						vs				(d)	(d)	(d)	(d)	(d)	(d)	(d)	(d)
TD-NiCr	Negligible	vs	s						w		(d)	(d)	(d)	(d)	(d)	(d)	(d)	(d)
TD-NiCrFe	Negligible	vs	s						w		(d)	(d)	(d)	(d)	(d)	(d)	(d)	(d)
Chromel A	Moderate	vs	m		a_o = 0.83 (8.30), vw			w(?)				vs		a_o = 0.83 (8.30), m				
Chromel AA	Light	s	s		a_o = 0.84 (8.40), m							w		a_o = 0.83 (8.30), vw				
Chromel C	Light	vs	m		a_o = 0.84 (8.40), w			w(?)				s		vw(?)				
Chromel P	Moderate	s	s		vw(?)							vw				vs		
DH-241	Moderate	vs	s		a_o = 0.84 (8.40), m			w(?)			w	s						
DH-242	Light	vs	m		a_o = 0.845 (8.45), s							s						
DH-243	Light	m	w		a_o = 0.845 (8.45), s			w(?)				m		a_o = 0.845 (8.45), vs				
DH-542	Light	s	s		a_o = 0.84 (8.40), v							m		a_o = 0.83 (8.30), vs		w(?)		
Tophet 30	Light	vw	vs									vs		w(?)				
DH-245	Light	m	s		a_o = 0.84 (8.40), s		w				(d)	(d)	(d)	(d)	(d)	(d)	(d)	(d)
IN-601	Moderate	m	s		a_o = 0.835 (8.35), w							vs		a_o = 0.84 (8.40), w				
IN-702	Light	vs			a_o = 0.845 (8.45), m	a_o = 0.82 (8.20), m(?)	s							a_o = 0.825 (8.25), s				
TD-NiCrAlY	Negligible	vs		vs			vw(?)		w		(d)	(d)	(d)	(d)	(d)	(d)	(d)	(d)
Hastelloy X	Light		m		a_o = 0.845 (8.45), s							s		a_o = 0.825 (8.25), vw				
HAS-C-276	Moderate	vs	s		a_o = 0.84 (8.40), s		w					s		vw(?)		m		
IN-600	Moderate	s	vs		a_o = 0.845 (8.45), w						vs			m				
L-605	Moderate	vs	m		a_o = 0.835 (8.35), vw							s		a_o = 0.82 (8.20), s		CuO(?) m		
HA-188	Light		s		a_o = 0.835 (8.35), s						vs			a_o = 0.825 (8.25), w				
HOS-875	Negligible	s		s							(d)	(d)	(d)	(d)	(d)	(d)	(d)	(d)
GE-1541	Negligible	s		s							(d)	(d)	(d)	(d)	(d)	(d)	(d)	(d)
GE-2541	Negligible	s		s							(d)	(d)	(d)	(d)	(d)	(d)	(d)	(d)
Multimet	Heavy		m		a_o = 0.85 (8.50), s							s		w(?)				

[a] Amount of collected spall: negligible, <0.25 mg/cm^2; light, 0.25 to 2.00 mg/cm^2; moderate, 2 to 10 mg/cm^2; heavy, 10 to 50 mg/cm^2.

[b] Relative pattern intensities: vs, very strong; s, strong; m, medium; w, weak; vw, very weak.

[c] a_o is the estimated spinel lattice parameter in nm (Å).

[d] No spall.

TABLE III. - X-RAY DIFFRACTION RESULTS AND SPALL CLASS RATING FOR ALLOY SAMPLES OXIDIZED FOR ONE-HUNDRED 1- HOUR HEATING CYCLES IN STILL AIR AT 1150° C

Alloy	Amount of spall[a]	Retained scale[b]								Spalled scale[b]							
		Solid solution	Cr_2O_3	αAl_2O_3	Spinel	NiO	SiO_2	ThO_2	Other	Solid solution	Cr_2O_3	αAl_2O_3	Spinel	NiO	SiO_2	ThO_2	Other
TD-Ni	Negligible					vs				(d)	(d)	(d)	(d)	(d)	(d)	(d)	(d)
TD-NiCr	Negligible	s	s					w		(d)	(d)	(d)	(d)	(d)	(d)	(d)	(d)
TD-NiCrFe	Negligible	vs	m					w		(d)	(d)	(d)	(d)	(d)	(d)	(d)	(d)
Chromel A	Light	s	m		a_o = 0.825 (8.25), s	vs					vs		vs(?)	vs			
Chromel AA	Light	m	w		a_o = 0.835 (8.35), s						w		a_o = 0.825 (8.25), s				
Chromel C	Light	w	m		a_o = 0.835 (8.35), s								a_o = 0.835 (8.35), s				
Chromel P	Massive					vs								vs	vs(?)		
DH-241	Light	m	s		a_o = 0.84 (8.40), vs					vs	s		a_o = 0.835 (8.35), s				
DH-242	Light	m	vs		a_o = 0.83 (8.30), w						vs		a_o = 0.825 (8.25), m				
DH-243	Light	vs	s		a_o = 0.835 (8.35), s					w	s		a_o = 0.845 (8.45), vs				
DH-542	Light	m	s		a_o = 0.835 (8.35), vw						vs		a_o = 0.845 (8.45), s				
Tophet 30	Light	v	vs		a_o = 0.835 (8.35), vw						vs		a_o = 0.825 (8.25), vw				
DH-245	Light	vs	m		a_o = 0.83 (8.30), m						w		a_o = 0.835 (8.35), s				
IN-601	Moderate	m	s		a_o = 0.83 (8.30), s					vvw	vs		a_o = 0.84 (8.40), vvw				
IN-702	Light	vs		w	a_o = 0.815 (8.15), s	w(?)					s		a_o = 0.835 (8.35), m				
TD-NiCrAlY	Negligible	vs		vs				m		(d)	(d)	(d)	(d)	(d)	(d)	(d)	(d)
Hastelloy X	Light		s		a_o = 0.835 (8.35), m		vw(?)						a_o = 0.825 (8.25), s	s			
HAS-C-276	Massive	s	vw		a_o = 0.83 (8.30), m		m						a_o = 0.825 (8.25), s				
IN-600	Massive	m	w		a_o = 0.83 (8.30), m		vs				w		a_o = 0.82 (8.20), s	s			
L-605	Massive	m	vw		a_o = 0.83 (8.30), s					m			a_o = 0.83 (8.30), vs				$CoWO_4$ s
HA-188	Heavy	vw	w		a_o = 0.83 (8.30), s		vw(?)						a_o = 0.825 (8.25), s				
HOS-875	Negligible	vs		s						(d)	(d)	(d)	(d)	(d)	(d)	(d)	(d)
GE-1541	Negligible	s		s					w	(d)	(d)	(d)	(d)	(d)	(d)	(d)	(d)
GE-2541	Negligible	s		vs					w	(d)	(d)	(d)	(d)	(d)	(d)	(d)	(d)
Multimet	Massive	(f)	(f)	(f)	(f)	(f)	(f)	(f)	(f)				a_o = 0.835 (8.35), vs				

[a]Amount of spall: negligible, <0.25 mg/cm^2; light, 0.25 to 2.00 mg/cm^2; moderate, 2 to 10 mg/cm^2; heavy, 10 to 50 mg/cm^2; massive, >50 mg/cm^2.

[b]Relative pattern intensities: vs, very strong; s, strong; m, medium; w, weak; vw, very weak.

[c]a_o is the estimated spinel lattice parameter in nm (Å).

[d]No spall.

[e]Because of severity of attack, test times were less than 100 hours.

[f]Sample completely oxidized.

TABLE IV. - GRAVIMETRIC AND THICKNESS CHANGE DATA FOR ALLOY TEST SAMPLES OXIDIZED IN STILL AIR FOR 100 HOURS OF CONTINUOUS EXPOSURE OR ONE-HUNDRED 1-HOUR CYCLES AT 1150° C

Alloy	Isothermal	Cyclic[a]	Isothermal		Cyclic		Nature of metal/oxide interface of cyclic sample at 250X
			Due to external scale	Plus grain boundary attack[b]	Due to external scale	Plus grain boundary attack[b]	
	Weight change at 100 hours, $\Delta W/A$, mg/cm^2		Thickness change (thickness measured from both sides), Δt, μm				
TD-Ni	11.63	13.87, 16.36	98	---	111	---	Smooth
TD-NiCr	[c]-0.27	-0.27	0	---	1	---	Smooth
TD-NiCrFe	[c]-0.18	-0.18	11	---	32	---	Smooth
Chromel A	1.85	-1.19, -4.42	(d)	15	27	120	Convoluted
Chromel AA	1.34	1.76, 2.89	3	40	4	150	Convoluted
Chromel C	2.20	1.70, 2.01	0	21	11	148	Convoluted
Chromel P	3.20, 2.95	[e]-80	27	---	774	---	Consumed
DH-241	2.63	-3.56, -4.39	(d)	15	12	61	Convoluted
DH-242	1.18	-0.26, -0.21	0	20	23		Smooth
DH-243	2.54	-4.46, -9.36	(d)	25	52	94	Convoluted
DH-542	1.45, 1.32	-1.52, -2.24	14	---	27	---	Smooth
Tophet 30	2.11	1.31, 0.46	(d)	7	37	---	Convoluted
DH-245	1.65	-0.43, -0.78	(d)	31	(d)	67	Convoluted
IN-601	4.10	-5.78, -19.33	20	89	15	110	Convoluted
IN-702	1.06	-2.08, -2.95	13	---	27	---	Smooth
TD-NiCrAlY	[c]0.72, [c]0.59	0.72, 0.59	16	---	11	---	Smooth
Hastelloy X	1.91, 2.06	-5.64, -6.46	9	71	28	169	Convoluted
HAS-C-276	2.46	[e]-629	31	---	1199	---	Smooth
IN-600	2.69	-95.72, -176.93	28	---	513	---	Smooth
L-605	3.28	-147.61, -211.45	71	181	366	513	Convoluted
HA-188	1.21	-19.46, -15.49	5	88	22	96	Convoluted
HOS-875	[c]0.95, [c]1.15	0.95, 1.15	9	---	23	---	Smooth
GE-1541	[c]1.41, [c]1.47	1.41, 1.47	38	---	35	---	Convoluted
GE-2541	[c]1.35, [c]1.38	1.35, 1.38	22	---	30	---	Convoluted
Multimet	12.67	[e]-680	92	---	2064	---	Consumed

[a]In $\Delta W/A$ results dual values are duplicate samples in different runs.

[b]General description, includes mostly grain boundary along with some internal oxidation.

[c]No detectable spall and low $\Delta W/A$ values; cyclic data used.

[d]External scale Δt difficult to differentiate from Δt due to grain boundary oxidation.

[e]Because of severity of attack, extrapolated from shorter time data.

TABLE V. - CLASSIFICATION OF SCALE CONTROL AND DERIVED RATE CONSTANT WITH VAPORIZATION CORRECTION FOR ISOTHERMAL SAMPLES OXIDIZED FOR 100 HOURS IN STILL AIR AT 1150° C

Oxide control category	Alloy	Parabolic scaling constant, k_p, $(mg/cm^2)^2/hr$	Paralinear fit[a]	Paralinear predictions		
				Time for maximum $\Delta W/A$, hr	Maximum $\Delta W/A$, mg/cm^2	Time ($\Delta W/A = 0$), hr
I - NiO control ($k_v \sim 0$)	TD-Ni	1.35	---	Vaporization not significant		
	Chromel P (0 to 1 hr)	2.40, 3.77	---			
II - Cr_2O_3 chromite spinel control ($k_v \sim 0.0081$)[b]	DH-242	0.036	Very good	175.9	1.26	709.7
	HA-188	0.037	Very good	181.5	1.30	732.30
	DH-542	0.42, 0.047	Very good	202.8, 229.5	1.45, 1.64	818.3, 926.0
	Chromel AA	0.043	Good	206.8	1.48	834.4
	DH-245	0.056	Very good	273.8	1.95	1104.7
	Chromel A	0.066	Fair	321.9	2.30	1299.1
	Hastelloy X	0.069, 0.077	Very good	337.1, 376.7	2.41, 2.69	1360.5, 1520.2
	Hastelloy-C-276 (2.5 to 100 hr)[c]	0.080	Fair	392.2	3.15	1575.1
	Tophet 30	0.080	Very good	390.4	2.79	1575.3
	Chromel C	0.085	Fair	415.6	2.97	1677.1
	DH-243	0.106	Very good	518.0	3.70	2090.2
	DH-241	0.112	Very good	547.0	3.90	2207.2
	IN-600	0.116	Very good	566.7	4.05	2286.8
	L-605	0.160	Very good	779.5	5.56	3145.7
	IN-702 (0 to 1.5 hr)	0.202	---	Vaporization with αAl_2O_3/ aluminate spinel overlayer insignificant		
	IN-601	0.232	Very good	1131.3	8.08	4565.8
	Multimet (0 to 15 hr)[d]	0.377	---	Vaporization masked by linear oxidation		
	Chromel P (1 to 99 hr)[e]	0.016, 0.016	---	Vaporization masked by linear oxidation		
III - αAl_2O_3 aluminate spinel control ($k_v \sim 0$)	HOS-875	[f]0.0096	---	Vaporization not significant.		
	TD-NiCrAlY	[f].0128(33 hr); $k_{p2} = 0.0014$	---			
	IN-702 (1.5 to 100 hr)	.020	---			
	GE-2541	[f].024(63 hr); $k_{p2} = 0.0074$	---			
	GE-1541	[f].025(63 hr); $k_{p2} = 0.011$	---			
IV - Cr_2O_3 with ThO_2 blockage control ($k_v \sim 0.012$)[b]	TD-NiCrFe	[g]0.0063	---	17.1	0.19	69
	TD-NiCr	[g].0068	---	14.1	0.16	57

[a]Paralinear fit - match seven time points with actual data ($\pm$ 0.15 mg/cm^2). Very good fit, 6 or 7 points match; good fit, 4 or 5 points match; fair fit, 2 or 3 points match.

[b]Rate of loss in $mg/cm^2/hr$ of Cr_2O_3 as CrO_3 vaporization.

[c]Oxidation rate linear for 0 to 2.5 hr; $k_l = 0.149$ $mg/cm^2/hr$.

[d]Oxidation rate linear after 15 hr; $k_l = 0.121$ $mg/cm^2/hr$.

[e]With NiO overlayer, Cr_2O_3 vaporization not considered significant.

[f]Based on slope of $(\Delta W/A)^2$-against-time plot, average of two runs.

[g]Based on downslope of ΔW-against-time plot, minimum limiting value.

TABLE VI. - AMOUNT OF METAL CONSUMED BY RETAINED, VAPORIZED, AND SPALLED OXIDES AS CALCULATED BY MASS BALANCE FOR 25 SHEET ALLOYS OXIDIZED IN STILL AIR FOR 100 HOURS AT 1150° C - ISOTHERMAL AND CYCLIC

Alloy	Isothermal oxide control category[a]	Isothermal					Cyclic				
		Retained[b]	Vaporized as CrO_3	Spalled[c]	Total	Calculated total metal consumed for one side[d], Δt_{W_m}, μm	Retained	Vaporized as CrO_3	Spalled	Total	Calculated total metal consumed for one side[d], Δt_{W_m}, μm
		Metal consumed, W_m, mg/cm^2					Metal consumed, W_m, mg/cm^2				
TD-Ni-CrAlY	III	0.74	0	0	0.74	3	0.74	0	0	0.74	3
TD-NiCrFe	IV	1.26	.81		2.07	3	1.26	.81		2.07	3
TD-NiCr	IV	1.27	.81		2.08	3	1.27	.81		2.08	3
HOS-875	III	1.18	0		1.18	4	1.18	0		1.18	4
GE-1541	III	1.62	0		1.62	6	1.62	0		1.62	6
GE-2541	III	1.54	0		1.54	6	1.54	0		1.54	6
IN-702	II→III	1.78(1)	~.01		1.79	4	1.78	.01	3.11	4.90	9
Tophet 30	II	5.78(1)	.55		6.33	9	5.78	.55	2.23	8.56	12
DH-242		3.76(1.5)			4.31	6	5.64		2.29	8.48	10
DH-245		4.78(1)			5.33	7	4.78		5.62	10.95	13
DH-542		4.21(2)			4.76	7	8.42		4.60	13.57	18
Chromel AA		4.11(3)			4.66	6	12.33		2.31	15.19	20
DH-243		6.71(1)			7.26	10	6.71		9.16	16.42	22
Chromel A		5.21(2)			6.76	8	10.42		6.68	17.65	22
Hastelloy X		5.51(2)			6.06	8	11.02		10.18	21.75	26
Chromel C		5.97(3)			6.52	9	17.91		5.20	23.66	30
DH-241		6.90(2)			7.45	10	13.80		9.28	23.63	31
IN-601		10.09(1)			10.64	15	10.64		16.66	27.30	38
HA-188		4.31(2.5)			4.86	7	10.78		21.16	32.49	40
TD-Nickel		51.20	0		51.20	57	51.20	0	0	51.20	57
IN-600		7.03(2)	.55		7.58	11	14.06	.55	149.05	163.66	199
L-605		8.33(3)	.55		8.88	12	24.99	.55	189.12	214.66	300
Chromel-P	I→II	13.16	~0		13.16	17	(e)	(e)	(e)	>280	---
HAS-C-276	?→II	6.53	.55		7.08	10	6.53	.55	455.06	462.14	518
Multimet	II→?	28.38	.55		28.93	40	(e)	(e)	(e)	>620	---

[a] I - NiO; II - Cr_2O_3/chromite spinel; III - αAl_2O_3/aluminate spinel; IV - ThO_2-blocked Cr_2O_3.

[b] Number in parenthesis denotes cyclic/isothermal thickness ratio of scales used to give retained cyclic value of W_m.

[c] No apparent spall during isothermal test.

[d] Δt_{W_m} = total $W_m \times 10/D_{met}$, where D_{met} is average metal density (g/cm^3) approximated from XRD results of scales.

[e] Consumed.

TABLE VII. - COMPARISON OF CYCLIC (ONE-HUNDRED 1-HOUR CYCLES) AND ISOTHERMAL OXIDATION RESULTS

FOR 25 SHEET ALLOYS IN STILL AIR AT 1150° C

Alloy	Isothermal oxide control category[a]	Isothermal parabolic rate constant, k_p, $(mg/cm^2)^2/hr$	Paralinear vaporization rate, k_v, $mg/cm^2/hr$	Amount of spall	Cyclic	Isothermal	Cyclic	Isothermal	Comments
					Thickness change (one side) estimated from mass balance, Δt, μm		Oxidation ranking[b] (based on area lost)		
TD-NiCrAlY	III	0.0128(33 hr); k_{p2} = 0.0014	~0	Negligible	3	3	Excellent	Excellent	All these alloys have negligible spalling because of thin αAl_2O_3 or Cr_2O_3 buildup. No spall-prone chromite spinel detected.
TD-NiCr	IV	0.0068	.012	↓	3	3	↓	↓	
TD-NiCrFe	IV	.0063	.012		3	3			
HOS-875	III	.0096	~0		4	4			
GE-1541	III	0.025(63 hr); k_{p2} = 0.011	~0		6	6			
GE-2541	II	0.024(63 hr); k_{p2} = 0.0074	~0		6	6			
IN-702	II – III	0.202 to 0.020 (1.5 hr)	0.008170 ~0	Light	9	4	Good	Excellent	No spall because aluminate spinel forms early.
Tophet 30	II	0.080	.0081	Light	10.5	9	Good	Good	30Cr favors Cr_2O_3 and delays spall-prone chromite spinel formation.
DH-242	II	.036	.0081	Light	11	6	Good	Excellent	Ni-20Cr-1Si, but 1 Nb appears to inhibit spalling.
DH-245	II	0.056	0.0081	Light	13.5	7	Fair	Good	All these alloys are basic Ni-(16 to 23) Cr-(0.03 to 2.0) Si heater type. Spalling is caused by increased chromite spinel buildup as compared with Cr_2O_3. In Hastelloy X, the 9 Mo tendency to vaporize as MoO_3 was apparently not involved.
DH-542	↓	.045	↓	↓	18.5	7	↓	Good	
Chromel AA		.043						Excellent	
DH-243		.106			21.5	10		Good	
Chromel A		.066			22	8		↓	
Hastelloy X		.073			26.5	8			
Chromel C		.085			30.5	9			
DH-241		.112			31	10			
IN-601	II	0.232	0.0081	Moderate	38	15	Poor	Good	Fairly high isothermal rate favors cyclic spall.
HA-188	II	.037	.0081	Heavy	39.5	7	Poor	Good	The Co-base alloy is a basic cyclic spaller, but La helps inhibit spalling.
TD-Nickel	I	1.35	~0	Negligible	57	57	Poor	Good	Since only NiO forms, spall is minimal but k_p is high.
IN-600	II	0.116	0.0081	Massive	190.5	11	Catastrophic	Good	All of these alloys are massive cyclic spallers because of their early heavy chromite spinel formation.
L-605	II	.160	.0081	↓	277	12	↓	Good	
Chromel P	I – III	3.09 to 0.016 (1 hr)	~0		387	17		Fair	
HAS-C-276	? – II	Linear to 0.080	.0081		519	10		Good	
Multimet	II – ?	0.377 to linear	.0081	↓	1032	40	↓	Poor	

[a] I - NiO; II - Cr_2O_3/chromite spinel; III - αAl_2O_3/aluminate spinel; IV - Cr_2O_3-ThO_2 blockage.

[b] Calculated area loss of 0.254-mm (0.010-in.) tensile sample: excellent, 0 to 5 percent; fair, 10 to 25 percent; poor, 25 to 50 percent; catastrophic, > 50 percent.

TABLE VIII. - SAMPLE SPECIFIC WEIGHT CHANGE FOR TYPICAL CYCLIC OXIDATION RUNS

[Six samples per run (two replicates per alloy); one-hundred 1-hr cycles at 1150° C in still air.]

Test time, hr	Furnace 1; average temperature, 1150° C			Furnace 2; average temperature, 1148° C			Furnace 3; average temperature, 1149° C		
	Test alloy								
	IN-702	GE-1541	TD-Ni	IN-702	GE-1541	TD-Ni	IN-702	HA-188	L-605
	Specific weight change, mg/cm^2								
8	-1.14 -1.35	0.63 .60	4.46 4.68	-1.22 -1.02	0.62 .64	4.99 5.70	-1.41 -2.02	1.04 .99	-1.28 -1.45
48	-1.62 -1.75	1.12 1.08	11.16 11.47	-1.72 -1.65	1.10 1.16	12.51 14.66	-2.00 -2.42	0.67 .91	-82.16 -90.09
100	-1.65 -1.85	1.42 1.45	16.36 16.75	-1.65 -1.68	1.44 1.47	18.31 21.85	-1.90 -2.31	-15.28 -13.13	-200.05 -225.55

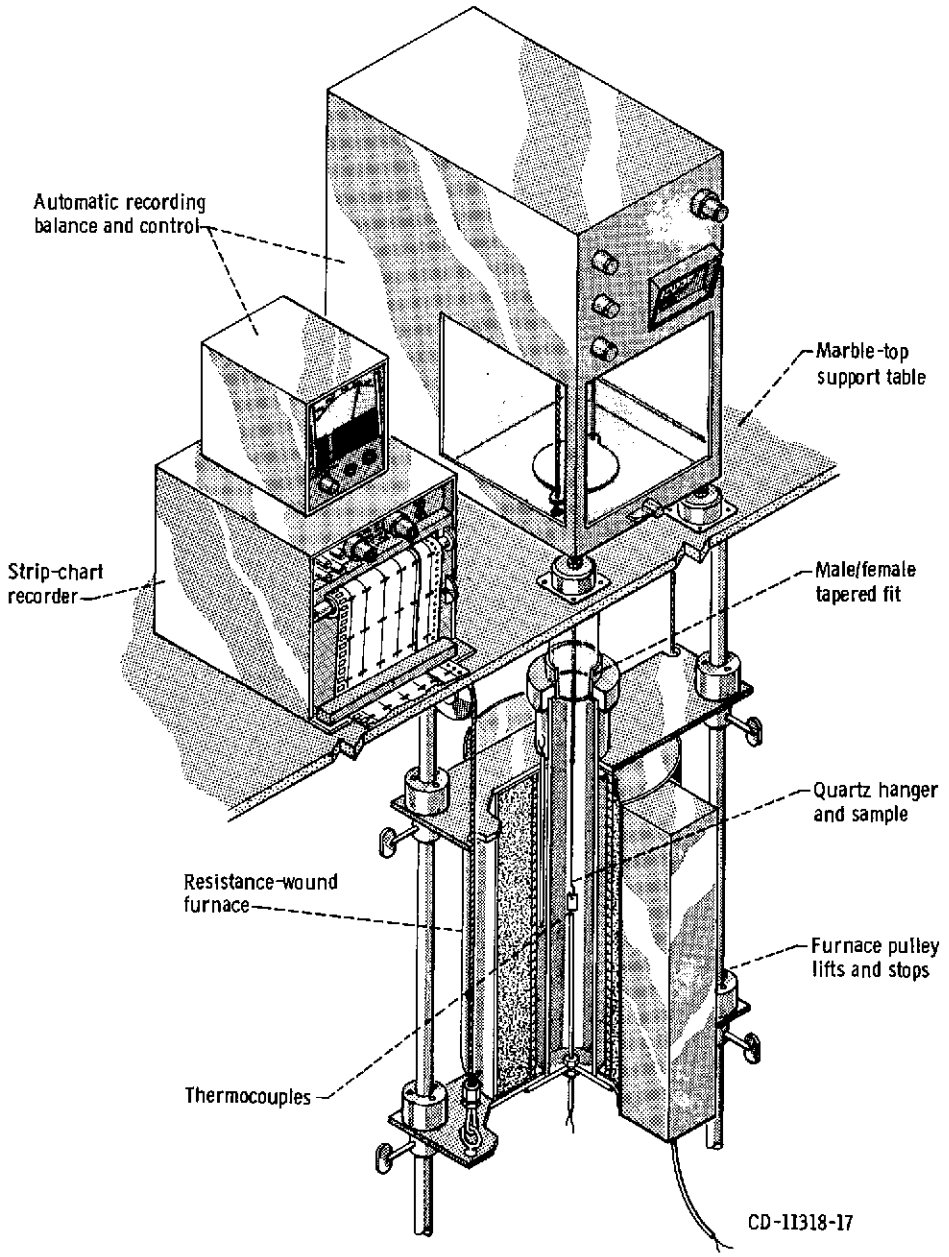

Figure 1. - Isothermal oxidation test apparatus.

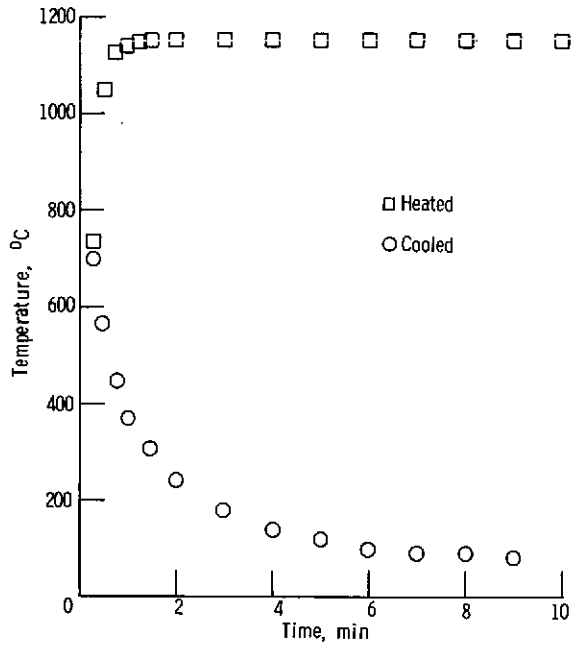

Figure 2. - Heating and cooling rate curves for cyclically heated and cooled sample (IN-702). Exposure temperature, 1150° C.

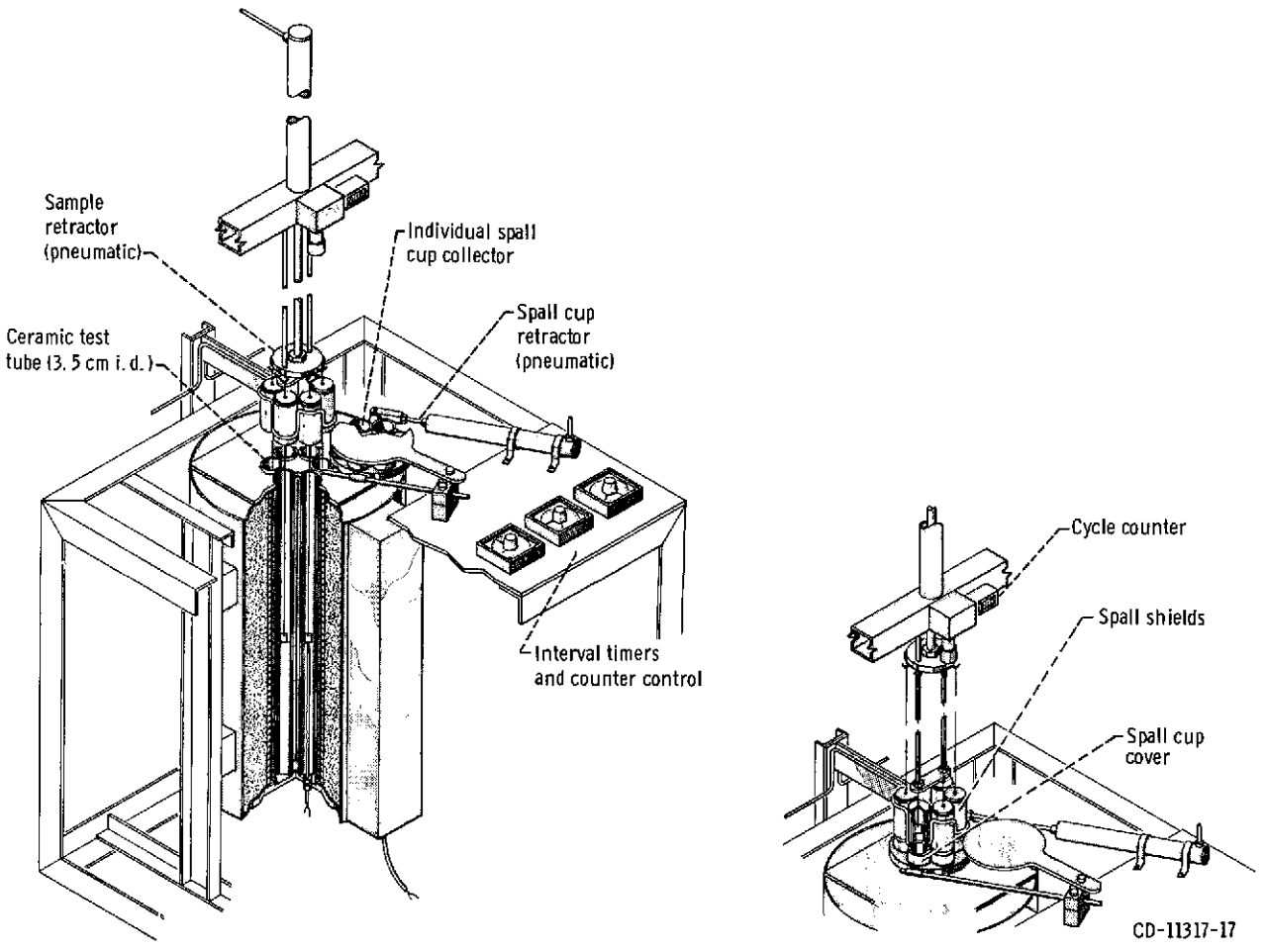

(a) Samples at test temperature.

(b) Samples cooled to ambient temperature.

Figure 3. - Multitube automatic high-temperature cyclic oxidation test apparatus.

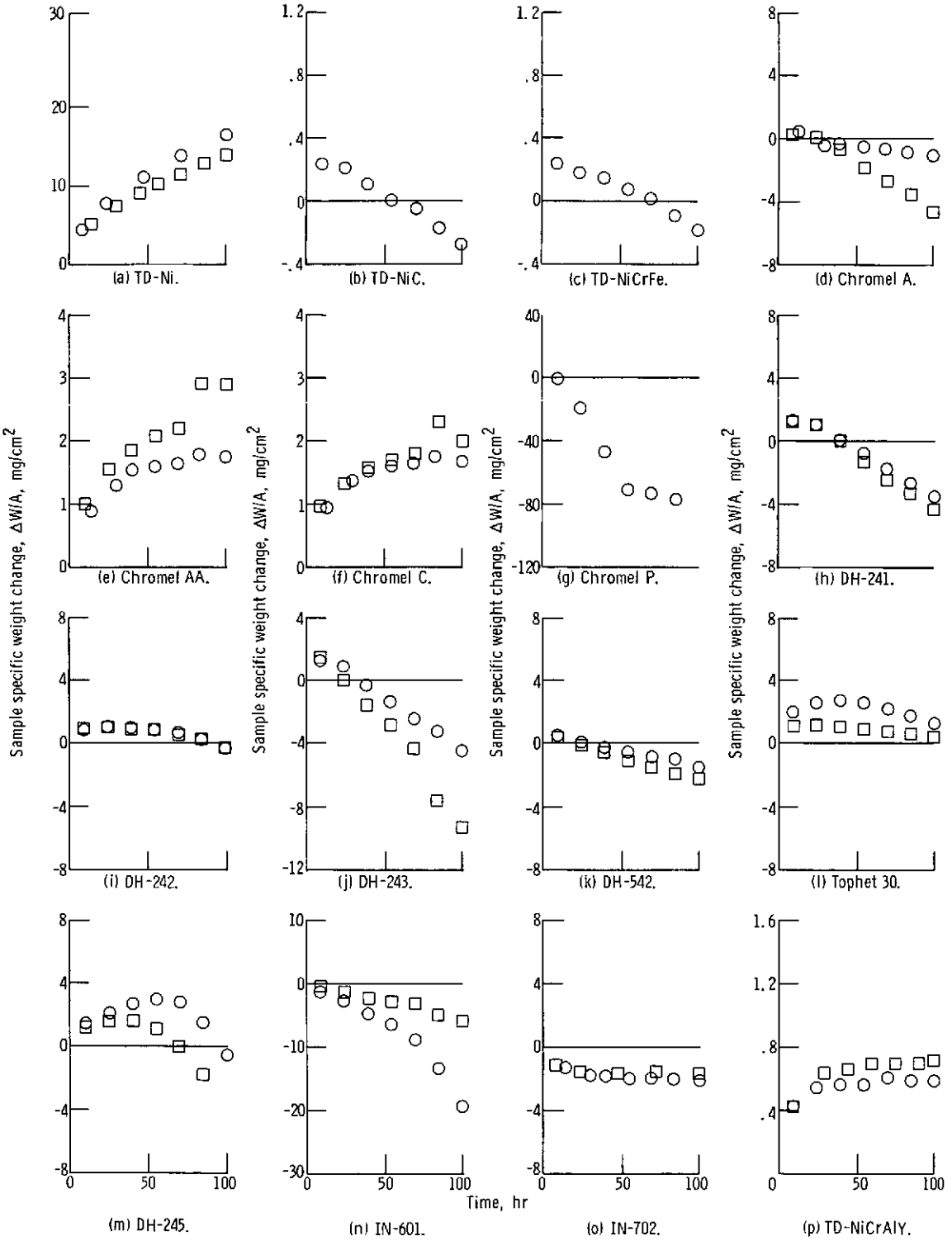

Figure 4. - Sample specific weight change as function of time for 25 alloys cyclically tested. One-hundred 1-hour cycles in air at 1150° C. Duplicate runs where noted.

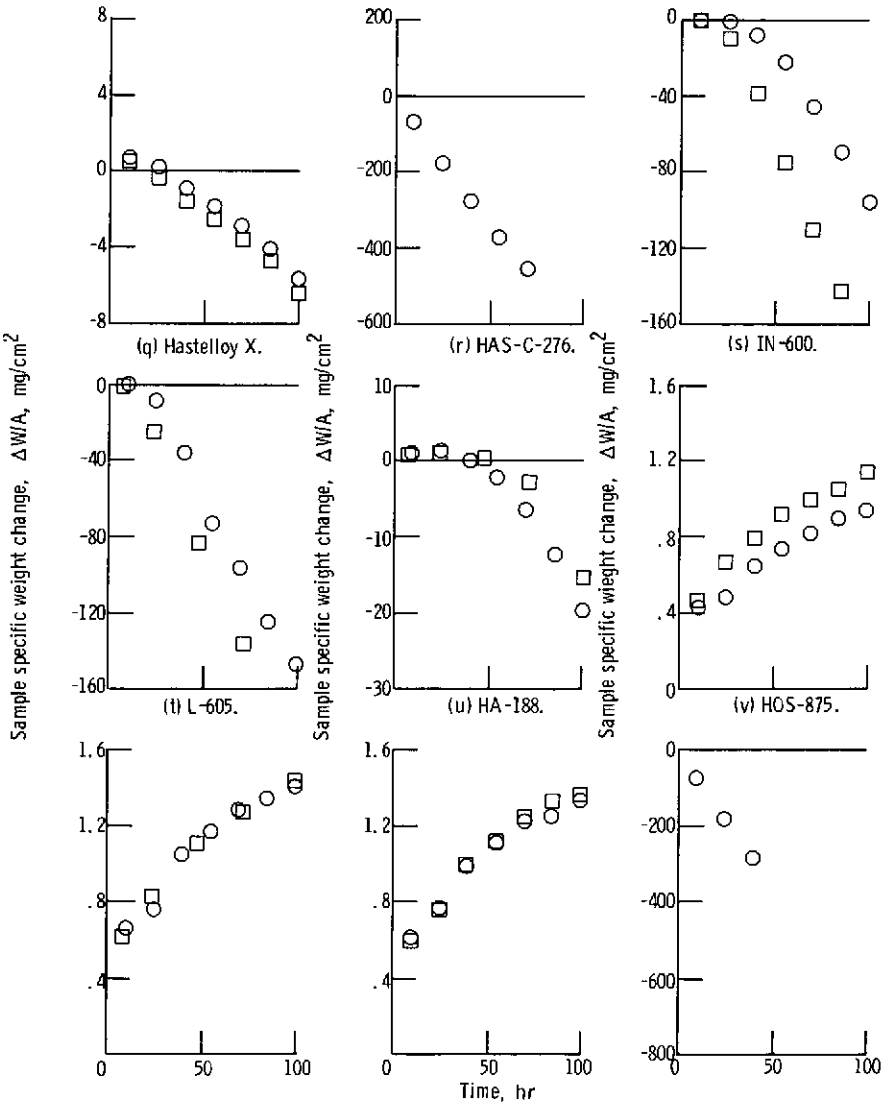

Figure 4. - Concluded.

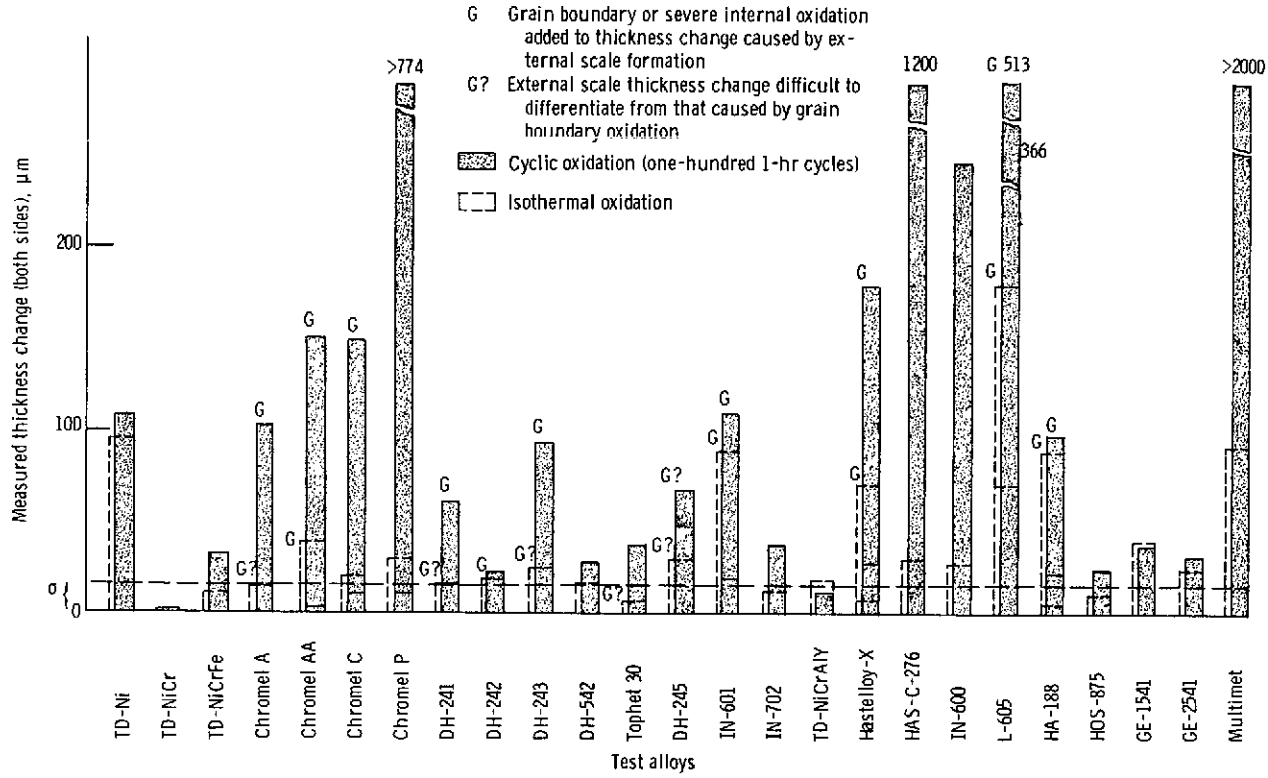

Figure 5. - Comparison of cyclic to isothermal oxidation of 25 alloys after 100 hours in still air at 1150° C, based on measured thickness change (both sides). Approximate measurement error, σ, 15 micrometers.

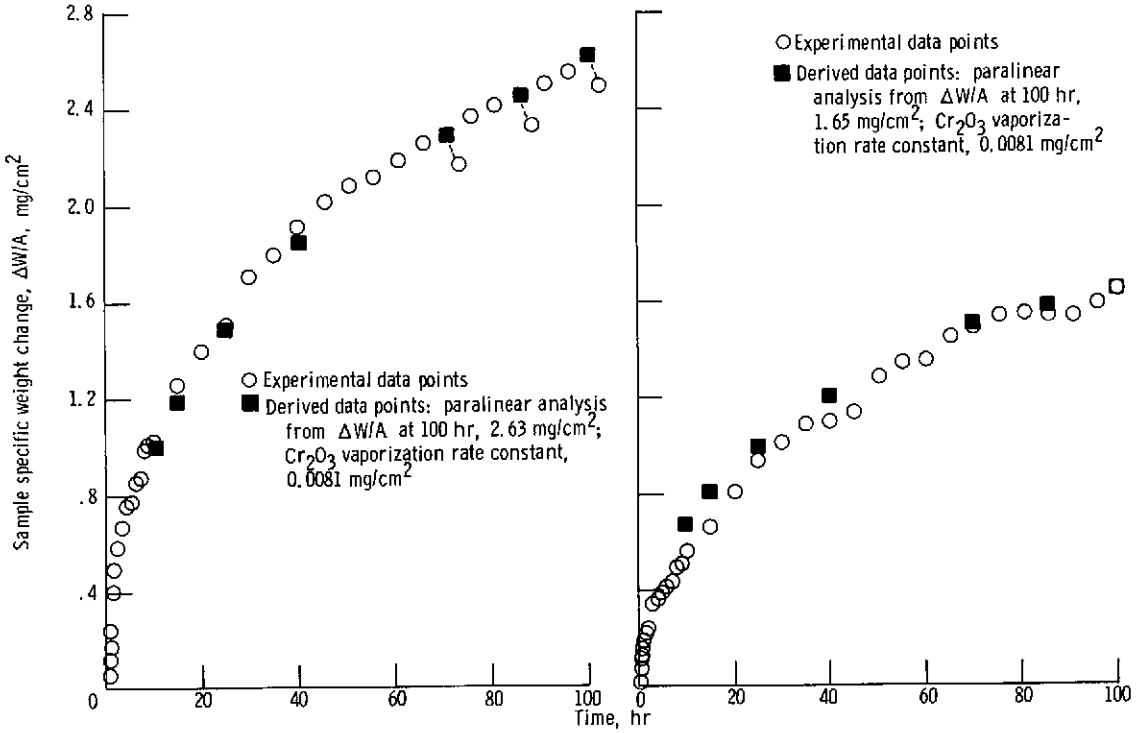

(a) DH-241. Very good fit, 7 out of 7 derived values within ±0.15 mg/cm² of actual data points.

(b) DH-245. Good fit, 6 out of 7 derived values within ±0.15 mg/cm² of actual data points.

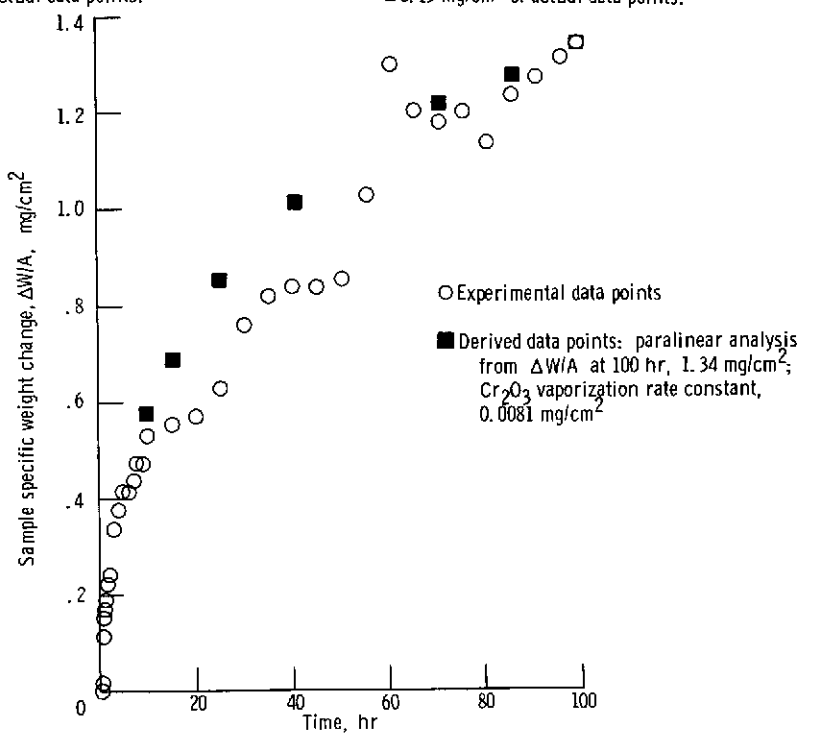

(c) Chromel AA. Good fit, 5 out of 7 derived values within ±0.15 mg/cm² of actual data points.

Figure 6. - Comparison of isothermal 1150° C oxidation data with paralinear predictions for still-air oxidation.

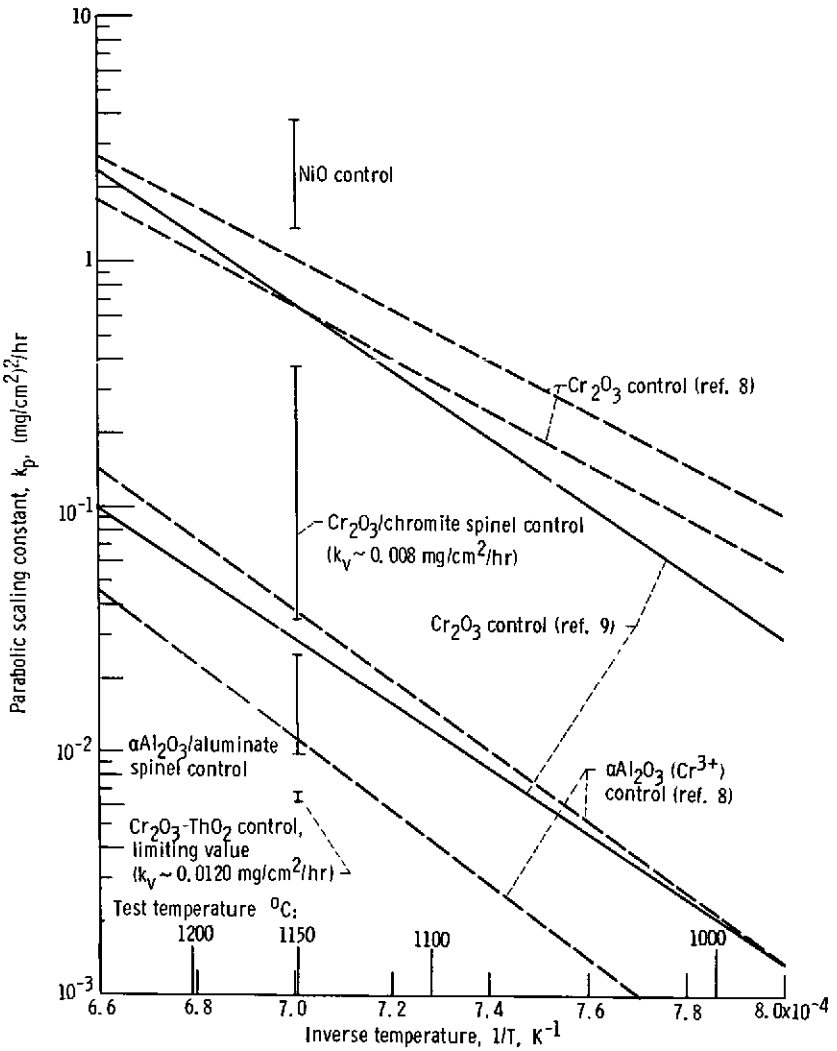

Figure 7. - Parabolic scaling constant as function of inverse temperature, showing the four types of isothermal oxidation control at 1150° C. Parabolic scaling constant k_p corrected for Cr_2O_3 vaporization; calculated vaporization rate constant k_v used for Cr_2O_3 loss rate.

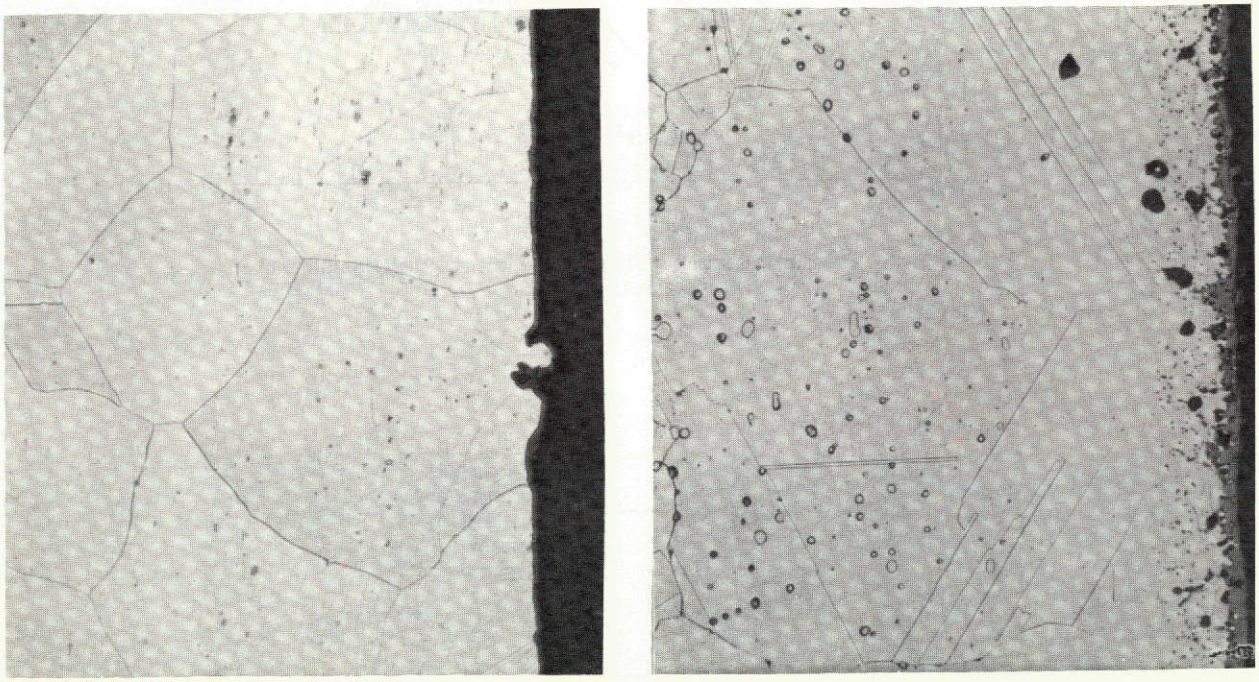

HOS-875

Hastelloy X

Figure 8. - Smooth (HOS-875) and convoluted (Hastelloy X) metal/oxide interfaces. Cyclic oxidation, one-hundred 1-hour cycles at 1150° C. Etch, $HCl + H_2O_2$. 250X.

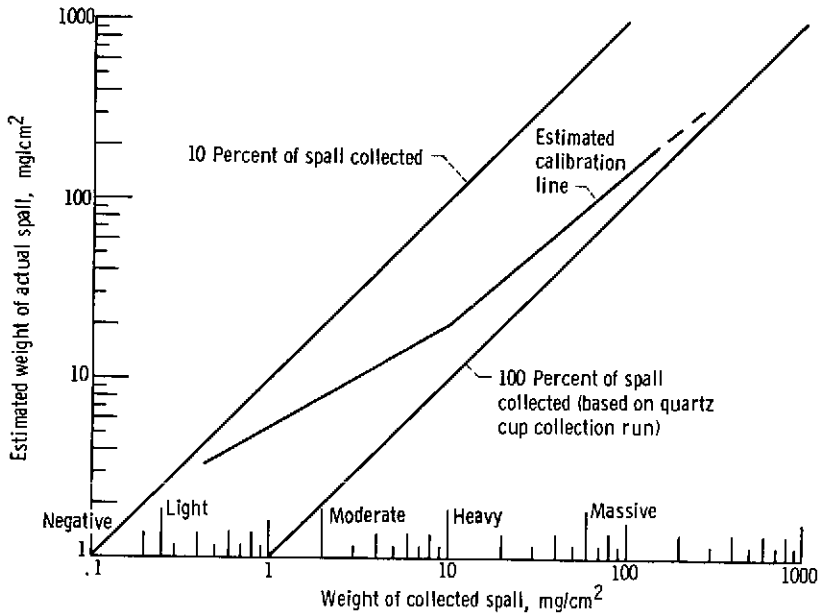

Figure 9. - Estimated true sample spall weight as function of collected spall weight - multitube cyclic oxidation apparatus.

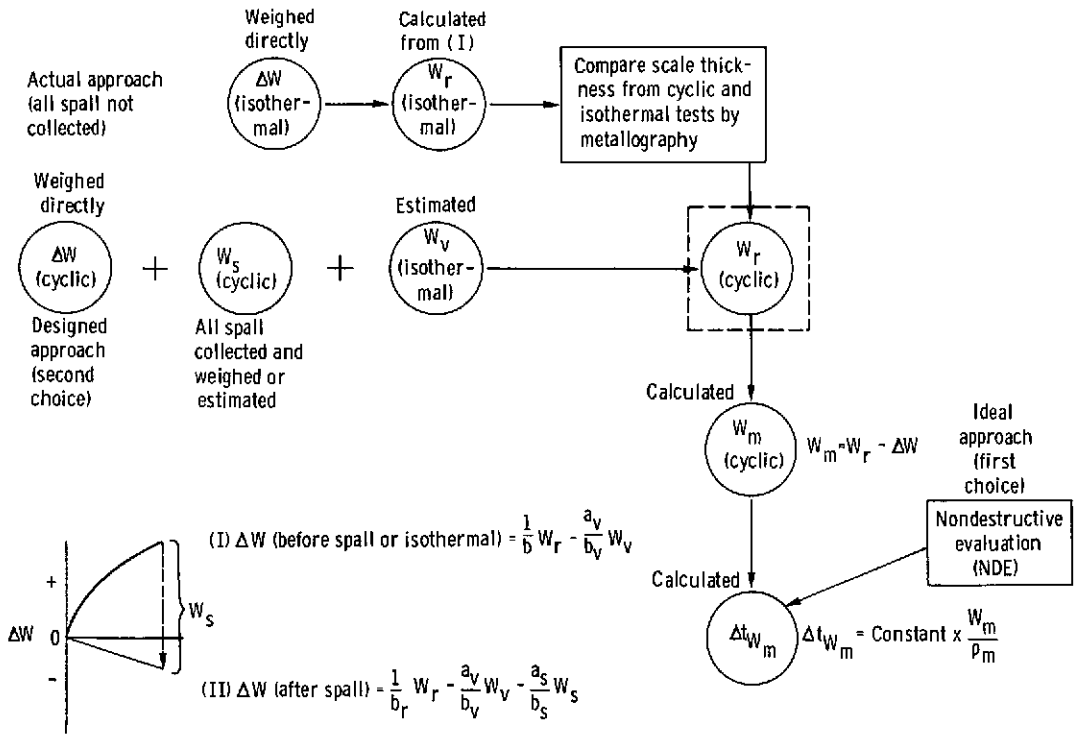

Figure 10. - Mass-balance approach for determining metal consumption including oxide vaporization and spalling.

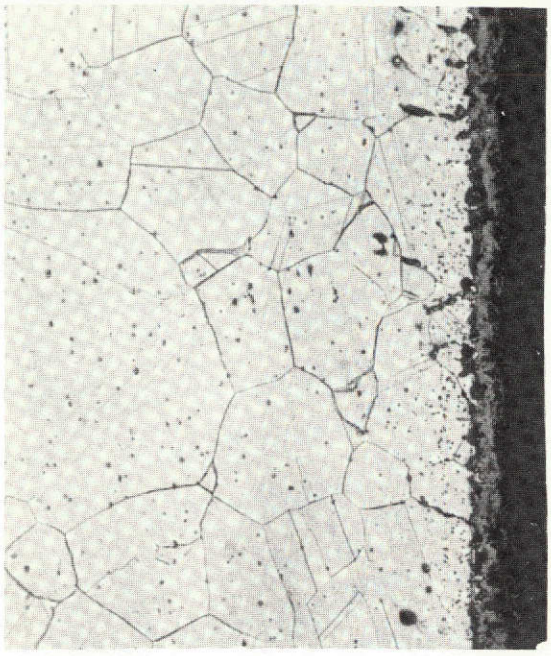

Tophet 30 (isothermal). Cyclic to isothermal retained scale ratio, ~1:1.

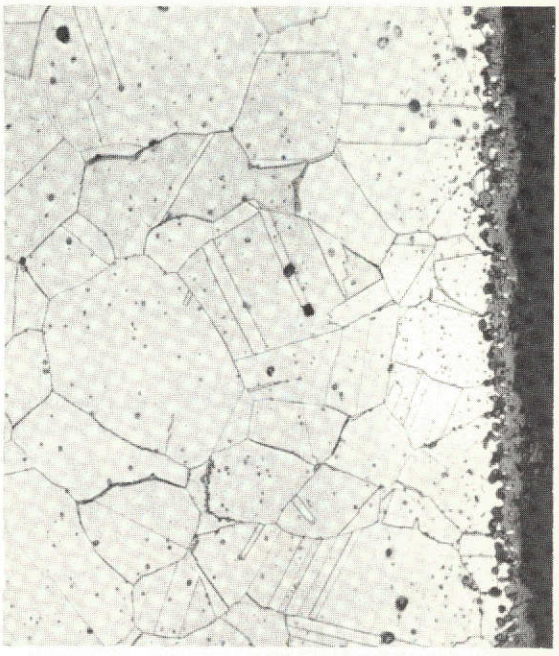

Tophet 30 (cyclic). Cyclic to isothermal retained scale ratio, ~1:1.

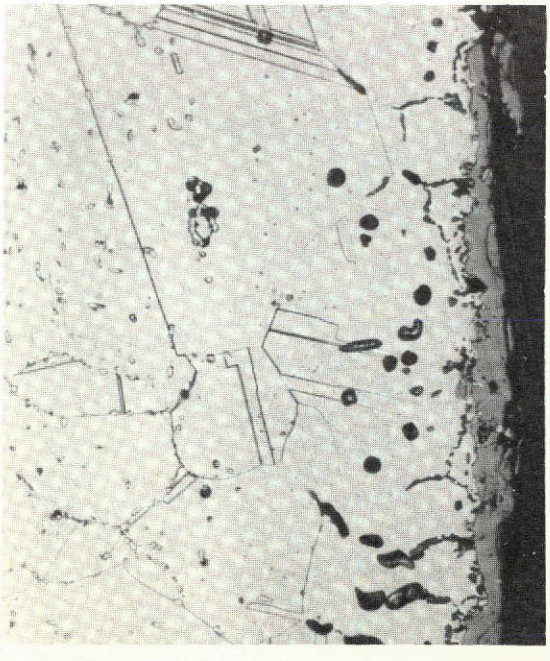

L-605 (isothermal). Cyclic to isothermal retained scale ratio, ~3:1.

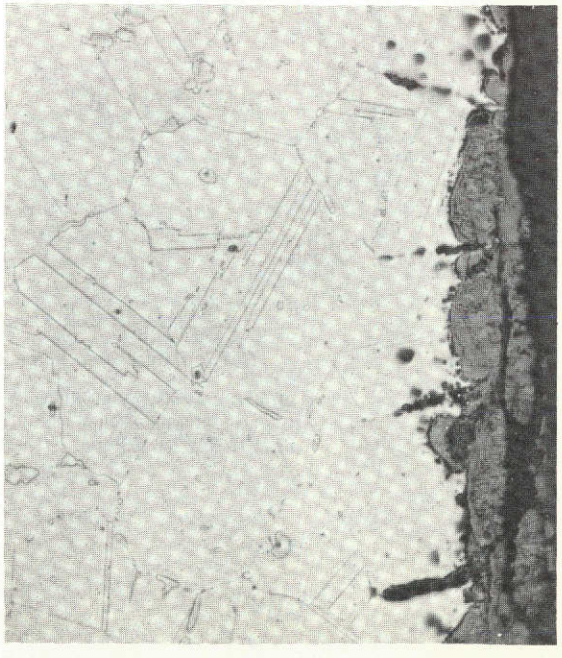

L-605 (cyclic). Cyclic to isothermal retained scale ratio, ~3:1.

Figure 11. - Comparative metallographic estimates of retained scale thickness for typical test samples after one-hundred 1-hour cycles and isothermal exposure in still air at 1150° C. Etch, $HCl + H_2O_2$. 250X.

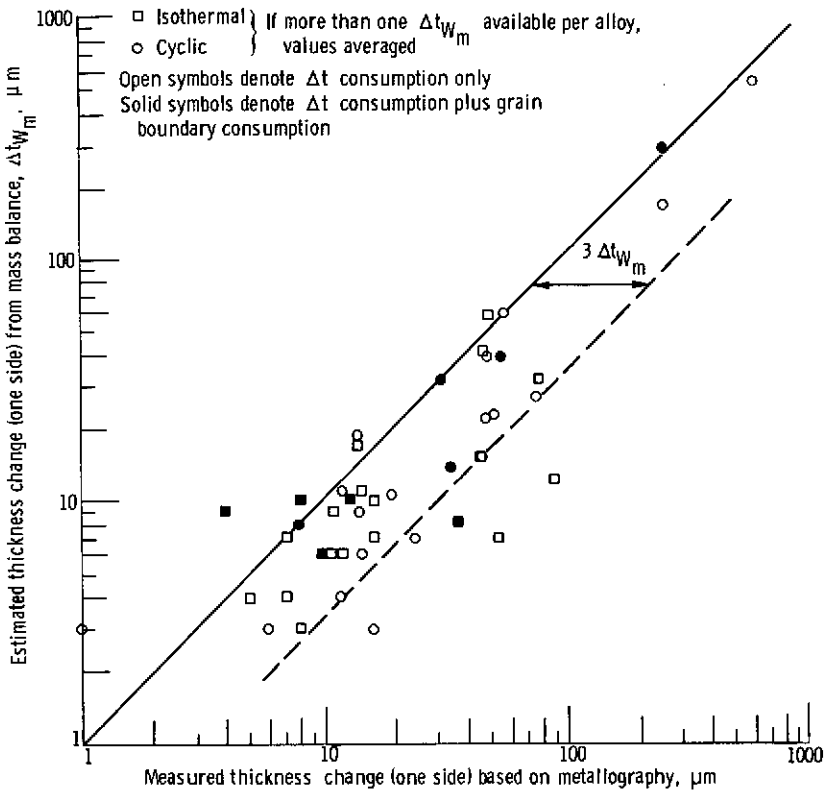

Figure 12. - Comparison of alloy thickness change calculated from a gravimetric mass-balance approach to actual measured thickness change for alloy oxidation in still air at 1150° C for 100-hour isothermal or one-hundred 1-hour cyclic exposures.

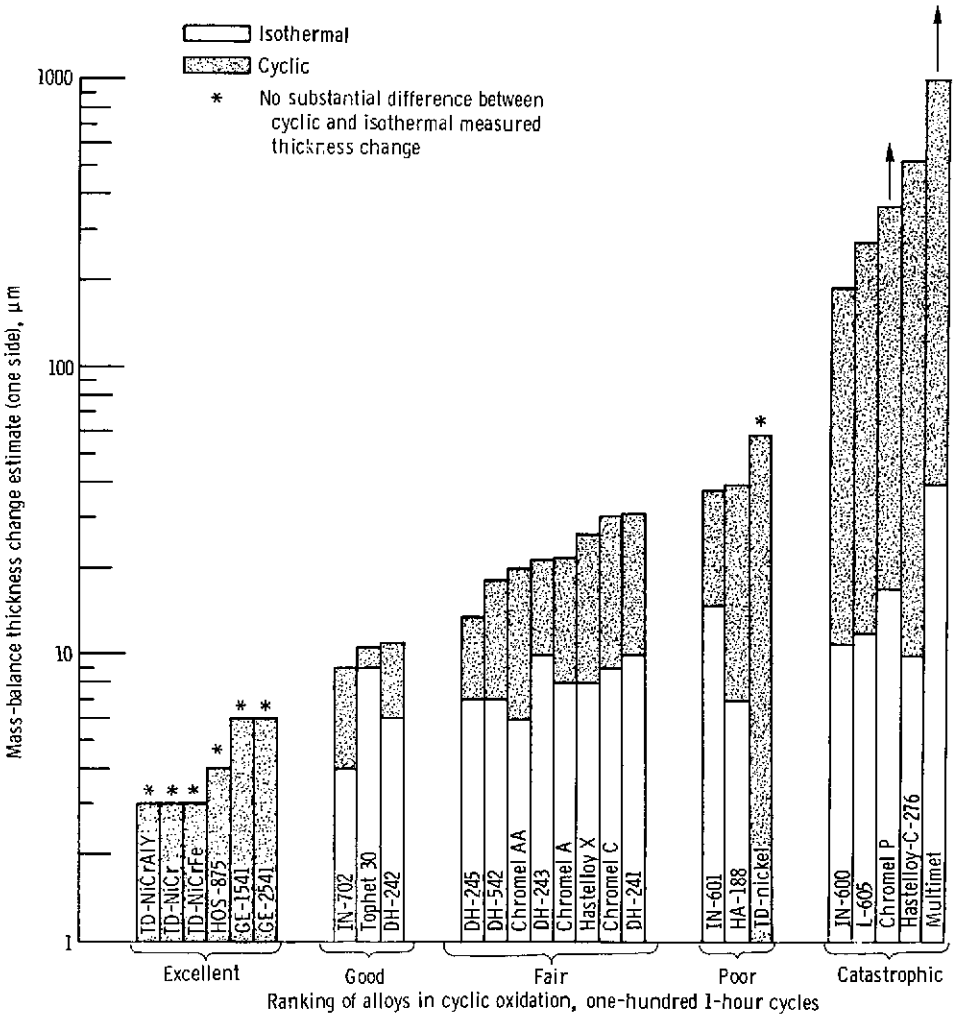

Figure 13. - Comparison of cyclic and isothermal oxidation for 100 hours in still air at 1150° C. Thickness change (one side) estimated from gravimetric data by mass-balance approach.

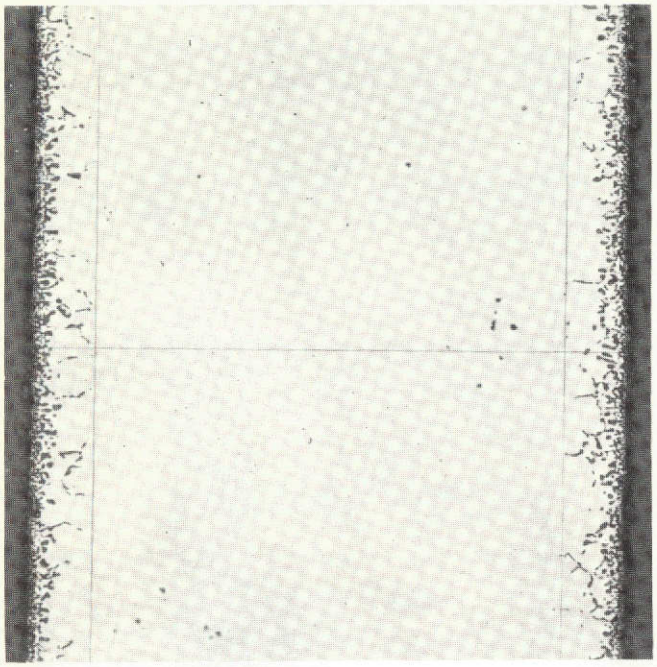

Cyclic. No etch. 100X.

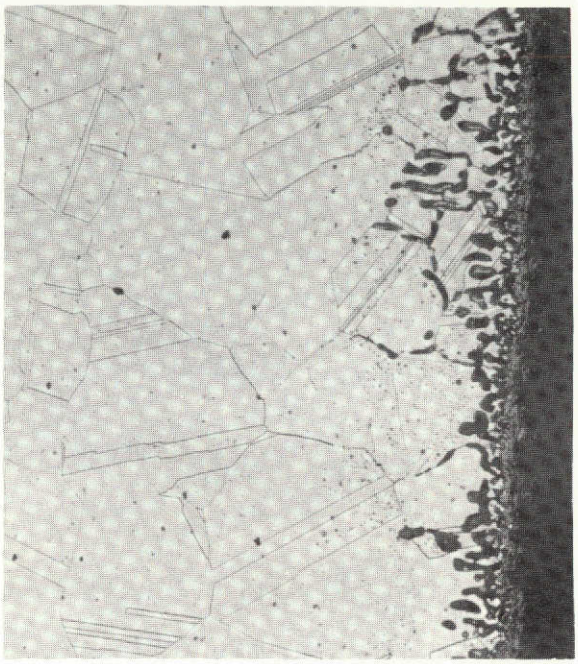

Cyclic. Etch, $HCl + H_2O_2$. 250X.

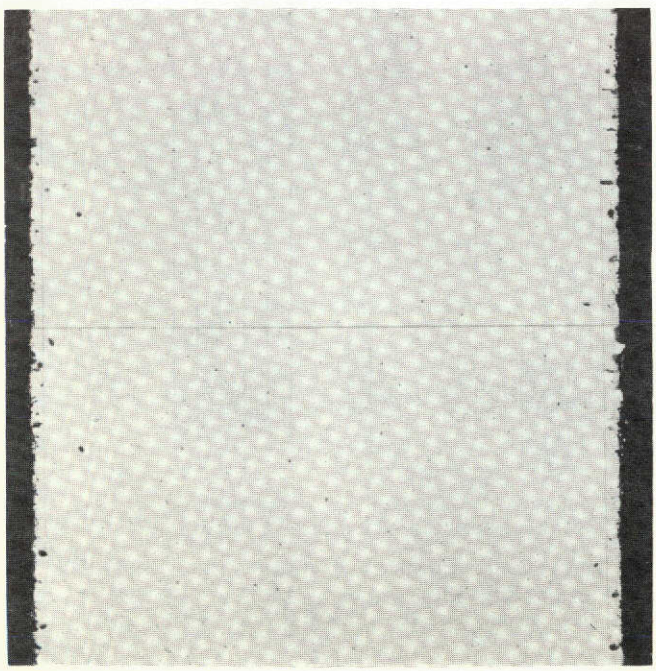

Isothermal. No etch. 100X.

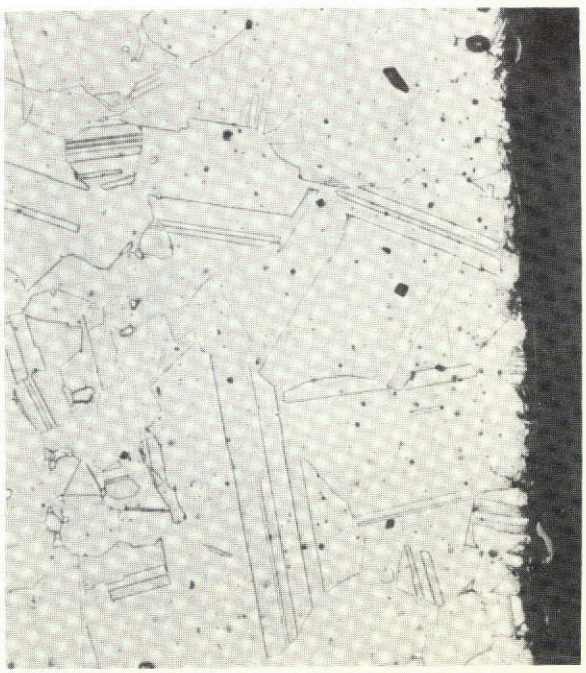

Isothermal. Etch, $HCl + H_2O_2$. 250X.

Figure 14. - Oxidation attack on Chromel AA after cyclic (1-hr cycles) and isothermal oxidation for 100 hours in still air at 1150° C.

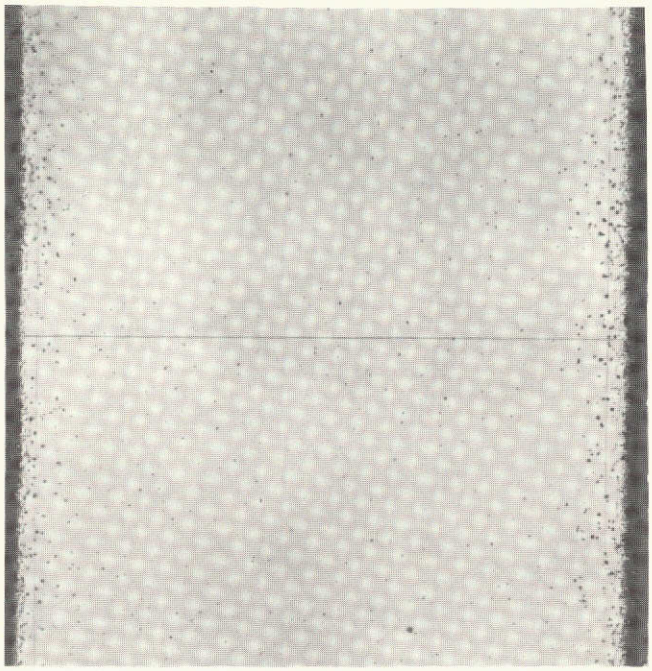

Cyclic. No etch. 50X.

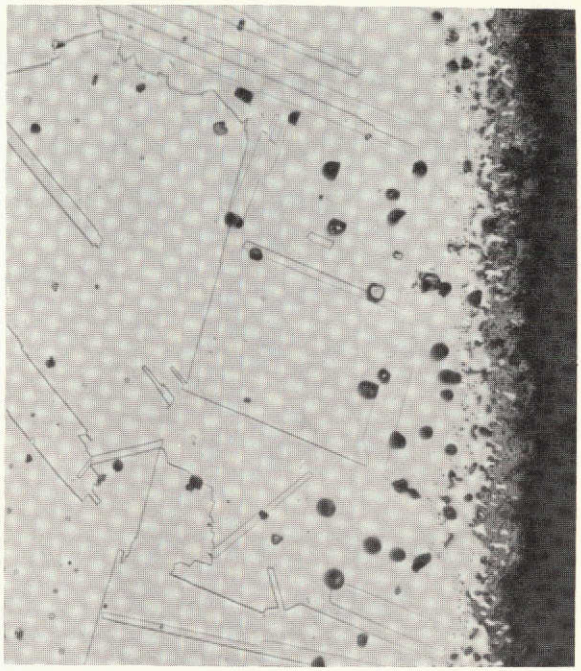

Cyclic. Etch, $HCl + H_2O_2$. 250X.

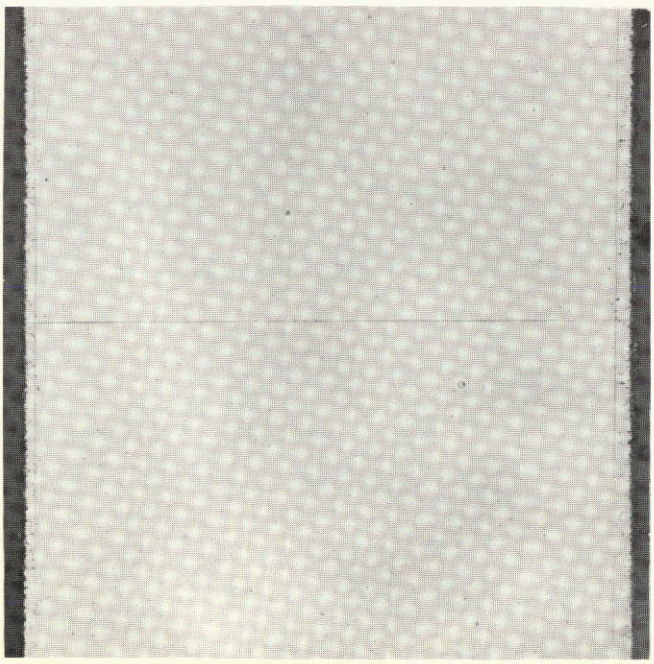

Isothermal. No etch. 50X.

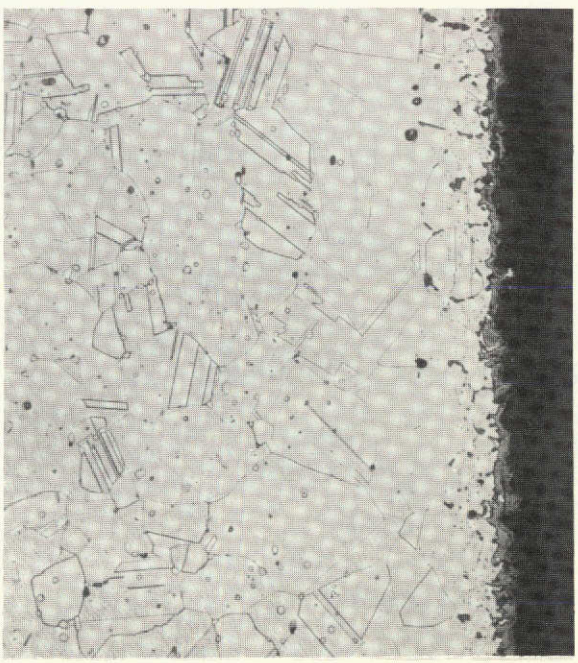

Isothermal. Etch, $HCl + H_2O_2$. 250X.

Figure 15. - Oxidation attack on HA-188 after cyclic (1-hr cycles) and isothermal oxidation for 100 hours in still air at 1150° C.